

University of Alberta

**BROADBAND SEISMIC ANALYSES OF THE CRUST AND NOISE SOURCES IN
ALBERTA, CANADA**

by

Luyi Shen

A thesis submitted to the Faculty of Graduate Studies and Research in partial fulfillment of the requirements for the degree of **Master of Science**

in

Geophysics

Department of Physics

©Luyi Shen
Spring 2013
Edmonton, Alberta

Permission is hereby granted to the University of Alberta Library to reproduce single copies of this thesis and to lend or sell such copies for private, scholarly or scientific research purposes only.

The author reserves all other publication and other rights in association with the copyright in the thesis, and except as herein before provided, neither the thesis nor any substantial portion thereof may be printed or otherwise reproduced in any material form whatever without the author's prior written permission.

Abstract

Cross-correlation of continuous seismic recordings has been proven effective in extracting the Green's function between two seismic stations. Travel-time and waveform source migration calculations jointly suggest a persistent noise source near Lesser Slave Lake (LSL), a large ice-covered lake in Alberta, Canada, during winter months. Subspace inversions of effective Green's functions from five narrow frequency bands (0.002-0.2 Hz) reveal low velocities in the upper crust beneath Alberta basin, which indicates strong effects from the thick platform sedimentary cover. Consistently low velocities are also observed beneath Wabamun domain but the areal coverage is considerably smaller than the published domain boundaries. The lower-crustal velocities beneath southern Loverna Block is 10% faster than the regional average. As the possible remnant cratonic core of the Hearne province, this northeast-striking anomaly extends to the western part of Medicine Hat Block and contributes to a strong east-west structural gradient in the latter domain.

Acknowledgements

I would like to express my gratitude to my fellow graduate students, Ahmet Okeler, Sean Contenti and Ryan Schultz for their insightful scientific suggestions and generous help to my research work. Also, I'm grateful to my friends in and outside of this department for their friendship and support which made the life in Edmonton much more enjoyable.

Above all, I thank Dr. Yu Jeffery Gu, who initially ignited my interests in Geophysics and supervised my research work as both undergraduate research assistant and graduate student. I wouldn't be able to present this thesis without Dr. Gu's help.

Contents

1	Introduction	1
1.1	Ambient Noise Correlation	1
1.2	Microseismicity from Ice Capped Large Water Body	3
1.3	Crustal Structure of Alberta	4
2	Microseismic Noise	8
2.1	Noise correlation and remote noise source	8
2.2	Local microseismic noise source	13
2.2.1	Travel Time Migration	13
2.2.2	Waveform Migration	17
2.2.3	Frequency Dependence of Noise Energy	22
2.3	Discussion	24
2.4	Conclusion	32
3	Noise tomography	33
3.1	Tectonic Setting	33
3.2	Data and Methods	37
3.3	Tomographic Results	46
3.3.1	Assessment of Data Resolution	46
3.3.2	Group Velocity Maps and Cross-sections	48
3.4	Discussion	51

3.4.1	Northern Alberta	52
3.4.2	East Alberta Orogen and Snowbird Tectonic Zone	58
3.4.3	Central Alberta	59
3.4.4	Southern Alberta	62
3.4.5	Rocky Mountains	65
3.5	Conclusions	66
4	Conclusion	69
4.0.1	Future direction and suggestions	71
A	Appendix	100
A.1	List of Abbreviations	100

List of Figures

- 2.1 Distribution of stations from the Canadian Rockies and Alberta Network (CRANE, black triangles) and nearby Canadian National Seismographic Network (CNSN, red diamond). The background colors show the topography of the region. The thin gray lines connecting the stations indicate all station pairs analyzed by this study. The blue lines with arrows indicate the station pair and order (e.g., for A B, the arrow would point to B) used in the migration analysis. The map inset shows the position of the study region relative to North America. Records from HYLO (available since June, 2010) are used for waveform comparisons in Figures 2.3 and 2.9. 9

- 2.2 (a) Stacked cross-correlation functions (color-coded and slightly interpolated) for all station pairs denoted by gray lines in Figure 2.1. The dashed lines indicate the theoretical lag time based on a constant background velocity of 3 km/s. The lag time-distance relationship approximately follows two linear move-outs, but significant asymmetry is present on the individual correlation functions. By our sign convention, a negative lag on the SCCF of A x B implies that Rayleigh waves reaches station A first. (b) Source migration result using all station pairs connected by gray lines in Figure 2.1. The color scale shows the magnitude of values (maximum=1); a high value implies a strong probability that the true source is located at the center of the grid point under discussion. (c) A magnified view of the study region enclosed by the rectangular box in Figure 2.2(b). A dominant noise source is observed in the Pacific Ocean southwest of the station array. 10
- 2.3 (a) Vertical component cross-correlation of station HON (anchor) and DOR for a cutoff frequency range of 0.01-0.2 Hz. The SCCF is computed by a series of narrow band-pass filters within the frequency range of interest. The move-out curve is symmetrical at both low and high frequencies but shows strong asymmetry in the range of 0.08-0.16 Hz. (b) Normalized absolute values of SCCFs of station pairs anchored by HON. The shaded region highlights the positive lag times, which roughly follow a semi-linear relationship. With the exception of HYLO, all SCCFs are used in regional source migrations. 14

2.4 (a) Time-migrated values of the study region. A cell with a large value implies a strong possibility of containing the true noise source. The maximum value is observed near LSL, though the precision of the noise source location is limited by station density. (b) values of station pairs based on a background Rayleigh wave group velocity of 3.0 km/s and hypothetical noise sources at the station locations of HON (green), CZA (red) and CLA (blue), respectively. As a simple example, for a hypothetical source at CZA (also the location of the anchor station) and station NOR (plotted as a red inverted triangle) is computed based on Equation (1) while assuming 1) , and 2) is the observed lag time of the SCCF between CZA (anchor station and hypothetical source) and NOR. The inverted triangles indicate station pairs with robust noise correlation peaks and stations that resulted in poor correlations with the majority of the three anchors (e.g., WALA) are omitted. c) Migration results based on background velocities ranging from 2.0 to 4.0 km/s. The vertical axis shows the distance between the resulting noise source location and reference point in east basin of LSL. The shaded region marks the range of realistic background velocities ranging from 2.5 to 3.4 km/s [Gu et al., 2011]. 15

2.5 Sample noise correlation stacks computed from REC (anchor) and five nearby stations. Low signal-to-noise ratios are observed on four stations, which reflects data quality issues. The final correlation pair provides additional information on the location of the potential regional noise source (see main text). 18

2.6	Result of waveform migration based on Equation (2). The individual SCCFs were filtered between 0.08 Hz and 0.16 Hz prior to migration, and the background Rayleigh wave group velocity was set at 3.0 km/s. Large migration amplitudes are observed near LSL, potentially extending to the western boundary of our study region.	20
2.7	Waveform migration results from four different Rayleigh wave group velocities. A local maximum is consistently observed in the vicinity of LSL. The estimated location uncertainty based on the movement of the source is 100-120 km. Effects of background velocity on source location are underscored by the large migration amplitudes near the northwestern boundary of the study region when falls below 2.7 km/s.	21
2.8	Waveform migration results from four slightly overlapping frequency bands. Strong migration amplitudes are observed near the west bay of LSL, particularly in the typical frequency range of ocean microseisms (0.06-0.18 Hz). The effect of the local noise source is minimal at longer periods (0.02-0.08 Hz, bottom right) as noise correlation functions become increasingly symmetric.	23
2.9	(a) Geographical location and path coverage provided by HON and four nearby stations. The solid and dotted lines with arrows indicate the expected source orientations based on the signs (all negative) and lag times of the SCCF maxima. (b) SCCFs computed for station pairs shown in Figure 9a based on recordings from 2007 to 2010. The high quality SCCFs show pronounced asymmetric correlation peaks with negative signs. In view of the unique geometries of these stations, a single local noise source must be present in the vicinity, preferably in the northwest, of HON.	25

2.10 (a) Seasonal variations of the SCCFs in 2008. This one-year data set is divided into two time periods (see main text) and the same correlation analysis is applied to each subset. In comparison with the summer months, the resulting SCCFs show much greater asymmetry during the winter of 2008. (b) Sample diurnal variations (for station pair HON and PER) during the winter months. The SCCFs are consistent between night and day, which suggest a common origin or mechanism. The 'signal' part of the SCCFs (-150 s to 0 s, bottom right) are more consistent than the 'noise' part of the SCCFs (-500 s to -200 s), top right) for the daily analysis. The amplitudes have been self-normalized for both time windows. (c) A schematic diagram illustrating the potential origins of microseismic noise. Mixing and resonance, as well as human activities and environmental processes, may be responsible for the asymmetrical SCCFs. 28

2.11 Mean wind energy during the winter (top panel) and summer (bottom panel) months of 2010 (see Data and Resources Section). Extreme values are observed along the Rocky Mountain front due to extreme topographic reliefs. Strong wind energy in the vicinity of LSL, which far exceeds those near water bodies of much greater sizes (e.g., Great Slave Lake, Athabasca Lake), could play a possible role in the generation of persistent local noise sources. 31

3.1	Distribution of stations (black triangles) from the Canadian Rockies and Alberta Network (CRANE) and nearby Canadian National Seismographic Network (CNSN). The dashed grey lines denote the known boundaries between tectonic blocks based on earlier geophysical and geological surveys [<i>Ross et al.</i> , 1991; <i>Villeneuve et al.</i> , 1993] The solid gray lines denote the vertical-cross sections in Figure 3.9 (see Section 3.4).	38
3.2	SCCFs computed for all station pairs. The peaks of the SCCFs increase linearly at an approximate speed of 3 km/sec.	39
3.3	(a) Unfiltered SCCF between station PER and HYO. The average of forward and time-reversed SCCF peaks represents the effective Green's function between the station pair. (b) Effective dispersion curves of SCCFs within the frequency range of 0.015-0.25 Hz. The lag times of the correlation peaks reflect the effect of Rayleigh wave dispersion.	41
3.4	Normalized waveform sensitivities for the five frequencies used in this study. The values are computed based on the reflectivity methods and a scaled regional P velocity model [<i>Kanasewich et al.</i> , 1995].	42
3.5	(a)-(e) Lag times of SCCF peaks for all five frequency ranges. The slopes of the linear plot are effective average velocities of the region at a given frequency, while the intercept of the least-squares fit shows the uncertainty of the average velocity and potentially biases in data quality and distribution. f) A comparison of the average velocities. The trend suggests increasing average crustal speeds with depth.	43

3.6	(a)-(e) Tradeoff curves of regularization factors (norm+Gradients) and model root-mean-squared (RMS) value. The regularization factors for the inversions are determined by the turning points. f) Reduction of data variance and RMS model velocities at all frequencies.	45
3.7	Resolution test for all five frequencies. The lower panels show the input checker-board pattern. The final SCCFs used for inversion are represented by the solid black lines connecting CRANE and CNSN stations (White triangles). A three sec white noise is added to the original model predicted values prior to inversions. Bigger grid-size ($1.5 \times 1.5 \text{ deg}^2$) is used for frequency ranges 0.002-0.04 Hz and 0.14-0.2 Hz due to limited numbers of quality SCCFs. Approximated 60% of the input amplitude is resolved for smaller grid size (a-c) while up to 90% of the input amplitude is resolved for the frequencies with coarser grid sizes (d and e).	47
3.8	Tomographic results of the SCCF group velocity inversions. Velocities for each of the five frequencies are plotted as perturbation to the average velocities. The black lines denote the reported boundaries between known tectonic blocks [Ross <i>et al.</i> , 1991]. CRANE and CNSN stations used in this study are represented by white triangles.	49
3.9	Estimated vertical cross-sections (see surface projection in Figure 1) of shear velocity perturbations relative to the regional averages. At a given depth, the contribution of a given frequency range is computed based on the corresponding sensitivity curve shown in 3.4.	53

3.10	Resolution tests based on hypothetical structures similar to the observed. (a) Results of a test that assumes an input high velocity anomaly between western MHB and Eastern MHB. The pattern is well resolved at frequency ranges of 0.10-0.16 Hz and 0.14-0.20 Hz. (b) Results of a test with an input high velocity structure across LVB and Vulcan structure. Both the amplitude and the oblique orientation of the input model is sufficiently recovered by the SCCFs at 0.002-0.04 Hz.	63
4.1	Anisotropy of crust. The anisotropy is quantified as $V_v - V_h$, while V_v is the velocity inverted from vertical component and V_h is inverted from radial component. The black lines denote the reported boundaries between known tectonic blocks [Ross <i>et al.</i> , 1991]. CRANE and CNSN stations used in this study are represented by white triangles.	73

Chapter 1

Introduction

1.1 Ambient Noise Correlation

As one of the rapidly expanding methodologies utilized by broad band seismic array, noise cross-correlation tomography gains its popularity by proving to be highly effective in interrogating crustal and upper-mantle structure in both regional and continental scale (eg., [Shapiro and Campillo, 2004; Sabra et al., 2005a; Huang et al., 2010; Dalton et al., 2011; Lobkis and Weaver, 2001]). Noise cross-correlation signals observed in different frequencies travels through different depths and therefore provide sensitivity through different layers of crust and upper-mantle. Thus, depth constraints could be extracted by observing surface wave signals through the waveform-frequency dispersion [Shapiro and Campillo, 2004; Shapiro et al., 2005]. Noise correlation function can retain travel time difference between stations from the persistent seismic noise source [Brzak et al., 2009]. Assuming ambient noise sources are perfectly randomly distributed around given station pair, cross-correlation results of continues recordings from stations yield the travel time difference between two stations, which translate to the effective Green's function result between two stations. Ambient noise-correlation experiments usually concentrate on periods between 5s to 50s, while longer periods signals were exploited for a larger scale experiment (eg., [Nishida et al., 2009]).

The theory of ambient noise correlation assumes the uniformity of seismic sources and absence of anisotropy [*Shapiro and Campillo, 2004; Sabra et al., 2005a*]. Though it's argued that most seismic noise is generated near surface and the modes which are more sensitive to the depth near surface would be excited in higher priority than that of lower depth, *Tsai [2010]* showed that partial Green's function between stations can be extracted even for modes induced by non-uniform layer structures.

The deployment of permanent and semi-permanent broad band seismic stations has emerged greatly in the past decade. Being sensitive to a wide frequency band (0.01-100Hz), the deployed seismic stations, such as US array (America) and Hi-net (Japan), provide exceptional data quality and successfully greatly facilitate seismic monitoring and structure imaging [*Gu, 2010*]. Geophysical studies in Alberta have benefited from the emerging usage of semi-permanent broad band seismic stations. By combining teleseismic and receiver function data, *Shragge et al. [2002]* first probed structures down to the middle mantle beneath Alberta's basement. It also raised unresolved questions about the assembly and evolution of western Laurentia.

Since 2006, the coverage of seismic data has been significantly improved by the deployment of the Canadian Rockies and Alberta Network (short named CRANE; [*Gu et al., 2011*]). This array of 13 semi-permanent stations is designed to complement the three existing CNSN stations and provide near-uniform receiver coverage in central and southern Alberta. The seismic recordings extracted from CRANE network facilitate a number of exciting research initiatives pertaining to the investigations of the Earth structure to [*Gu et al., 2011; Contenti et al., 2012*], to seismic sources [*Stern and Gu, 2011; Gu and Shen, 2012*]. This study concentrates on ambient seismic noise observations that provide the empirical Green's functions between stations through cross correlations. By exploring frequency-dependent wave velocities, we aim to provide a broadband, seismological snapshot of ambient

microseismic sources (Chapter 2) and the present-day domain structures/boundaries down to upper mantle depths (Chapter 3). While our interpretations require further verification or validation, the outcomes of this study offer new and potentially critical constraints on regional seismicity along with tectonic evolution of the western North America.

1.2 Microseismicity from Ice Capped Large Water Body

For over a half century, ocean swells and shoreline-wave interactions have been known to produce detectable seismic energy in the frequency range of 0.05-0.2 Hz [Longuet-Higgins, 1950; Gutenberg, 1951; Hasselmann, 1963]. These microseismic signals often exhibit strong directivity and, in some areas, seasonal or daily fluctuations [e.g., Schulte-Pelkum et al., 2004; Rhie and Romanowicz, 2006; Gerstoft and Tanimoto, 2007; Webb, 2007; Kedar et al., 2008; Yao and van der Hilst, 2009; Arduin et al., 2011; Schimmel et al., 2011]. Distinctive amplitude asymmetries in the cross-correlation function of seismic noise [Paul et al., 2005; Gu et al., 2007; Yang and Ritzwoller, 2008] have revealed key characteristics of source distribution, geometry, strength, and mechanism [Stehly et al., 2006; Brzak et al., 2009; Koper et al., 2010; Schimmel et al. 2011].

Pressure fluctuations in large rivers and lakes are also capable of generating sustained seismic signals. Lynch [1956] documented the passage of storms over the Great Lakes as a potential seismic source, radiating from the lake to distances as far as North Carolina. The frequencies of the lake wave during the summer time were consistent with that of the secondary (0.2 Hz) ocean microseism. Wind-induced lake wave microseisms (1-3 Hz) were later reported near Great Slave Lake [Weichert and Henger, 1976] and Lake Ontario [Kerman and Mereu, 1993], showing strong spectral correlations between buoy and on-land seismic records. River dis-

charge [Burtin et al., 2009] and gravitational variations associated with bed load transport near Geysers [Tikku et al., 2006] are alternative sources and mechanisms for localized seismic signals. Similar to oceanic wave sources, motions inside lakes and rivers are highly sensitive to fluid/mass discharge, water depth, shoreline steepness/geometry and bottom topography [Malm, 1999; Kvrarnas, 2001; Wuest and Lorke, 2003; Burtin et al. 2008]. For large ice-covered lakes, luminosity, snow coverage, ice thickness, and resonance are also contributing factors to ground motion [e.g., Patterson and Hamblin, 1988; Kenney, 1991, 1996; Rogers et al., 1995; Kelley, 1997; Petrov et al., 2007].

In Chapter 3 we will investigate the nature of persistent ground motions in the southwestern portion of the Western Canadian Sedimentary Basin (WCSB). Our observations reveal a local microseismic noise source near Lesser Slave Lake (LSL). The seasonal variation of the observed signals suggests potential ground motion within and around the closed water environment, i.e., a frozen lake. The existence of the observed noise source and its potential connection to human or environmental factors will be carefully examined.

1.3 Crustal Structure of Alberta

The basement structure under central/southern Alberta and northern Rockies contain vital records of the Precambrian tectonic development of western Laurentia and more recent interactions between the North American Craton and Cordilleran Orogen [Hoffman, 1990, 1988; Ross et al., 1991; Villeneuve et al., 1993; Ross, 2000]. Largely buried under a veneer of Phanerozoic sediments in the southern Western Canada Sedimentary Basin (WCSB), surface exposure of this region is confined to northeastern Alberta where significant geochemical signatures from the Archean Slave province have been identified to date [Hoffman, 1988; Burwash et al., 2000;

Ersan et al., 2009; *De et al.*, 2000; *Frost and Burwash*, 1986; *Canil et al.*, 2003]. In comparison, central and southern Alberta (the main focus of this study) are much less accessible. As an integral part of the western Canadian Shield (or Laurentia), this region underwent Archean and Proterozoic collisions among Hearne, Rae, Superior and Wyoming provinces, as well as latter-stage reworking [*Ross and Eaton*, 2002; *Aulbach et al.*, 2004; *Mahan and Williams*, 2005; *Beaumont et al.*, 1994] and sedimentation. The extensive collisional history resulted in a diverse geological framework of Archean craton(s), Proterozoic orogen(s), and associated accretionary margins known as "terranes". Detailed knowledge of this gradient zone between craton(s) and terranes [*van der Lee and Frederiksen*, 2005; *Marone and Romanowicz*, 2007; *Courtier et al.*, 2010; *Yuan and Romanowicz*, 2010], which defines the western boundary of Canadian Shield (or Laurentia), can provide critical insights on the assembly and evolution of the North American lithosphere. The intricate domain structure beneath southern WCSB has been investigated by regional gravity, magnetic, and seismic surveys [*Ross et al.*, 1991; *Ross*, 2000; *Thériault*, 1992]. Among the various approaches, the use of reflection seismic methods has been particularly effective at mapping the velocity, faults and reflecting interfaces in the crust. In the early 1990s, a series of active-source seismic surveys were conducted as part of LITHOPROBE project [*Ross*, 2000]. The Alberta Transect from this trans-Canada experiment contains three major reflection profiles that totalled 1400 km in length [*Ross*, 2000; *Lemieux et al.*, 2000; *Eaton et al.*, 1999a; *Dietrich*, 1999]. Additionally, reflection and refraction analysis based on Alberta Basement Transect (ABT), Deep Probe, and Southern Alberta Refraction Experiment (SAREX) [*Clowes et al.*, 2002; *Gorman et al.*, 2002] enabled verification and refinement of the theories [*Hoffman*, 1988] regarding the basement formation and evolution of the ectonic domains in southern WCSB [*Bouzidi and Schmitt*, 2002; *Eaton et al.*, 2000, 1999a,b; *Eaton and Cassidy*, 1996; *Lemieux et al.*, 2000; *Ross and Eaton*,

2002; Ross *et al.*, 2000, 1995; Ross and Eaton, 1997; Zelt and Ellis, 1989; Zelt and White, 1995]. Complementary broadband seismic recordings from Canadian National Seismic Network (CNSN) stations [Cassidy, 1995; Eaton and Cassidy, 1996] and temporary deployments such as Canadian Northwest Experiment (CANOE) [Mercier *et al.*, 2008; Dalton *et al.*, 2011], the BATHLOITH project [Mercier *et al.*, 2009] and Florida-to-Edmonton Array (FLED) [French *et al.*, 2009] offered continuous data constraints down to upper mantle depths. Analysis of broadband, teleseismic data (e.g., [Shragge *et al.*, 2002; Mercier *et al.*, 2008, 2009]) shed new lights on the current state as well as dynamic history of the region. For instance, the body-wave tomography and shear wave splitting measurements from [Shragge *et al.*, 2002] raised important questions on the integrity of the lithosphere beneath central Alberta.

Progress aside, limited surface exposed geology in southern WCSB presented a formidable challenge to the assessment of regional basement history. It highlights the need for indirect seismic interrogation methods that, until recently, had been emphasized in the southern WCSB due to linear receiver formations and the short durations of the active- or passive-source experiments. Only local-scale, two-dimensional (2D) receiver geometries had been attempted [Kanasewich *et al.*, 1995], while the vast majority of the aforementioned experiments lasted for 1 year or less (with the exception of three permanent CNSN stations EDM, WALA and SLEB). These apparent drawbacks left much of the southern WCSB under-sampled. Consequently, interpretations of the boundary and vertical extent of the domains in southern WCSB leaned heavily on EM and potential field observations (e.g., [Hope and Eaton, 2002; Ross *et al.*, 1991, 2000; Boerner, 1999]), which suffered from low depth sensitivity and their relationship with seismic velocities are not well-established. Chapter 3 will carefully examine the ambient seismic noise records and provide a broadband , seismological perspective of the domain formation and

history in western Laurentia.

Chapter 2

Microseismic Noise from Ice Covered Lake

2.1 Noise correlation and remote noise source

This study utilizes continuous records from CRANE [Gu et al., 2009], the first semi-permanent broadband seismic array in Alberta, in combination with three stations from the Canadian National Seismograph Network (CNSN). Most of these receivers (Figure 2.1) operated continuously between 2007 and 2008 and provide the first semi-uniform array coverage in the southern-central WCSB. The average distance between stations is approximately 180 km, which translates to a shear wave travel time of 60 s at an average crustal speed of 3 km/s. We include additional data from 2009-2010 for improved resolution and support of key findings. For each station, we divide continuous displacement seismograms into 12-hour intervals and apply a Butterworth band-pass filter with cutoff frequencies of 0.01 Hz and 10 Hz. The resulting vertical-component seismograms for each station pair are correlated and stacked over spans of 5+ months [e.g., Yang et al., 2007; Bensen et al., 2007; Brzak et al., 2009].

A lag-time vs. distance diagram based on all stacked cross-correlation functions (SCCFs) shows energetic signals resulting from propagating Rayleigh waves [e.g., Schulte-Pelkum et al. 2004; Shapiro et al., 2005, 2006; Stehly et al., 2006; Gerstoft

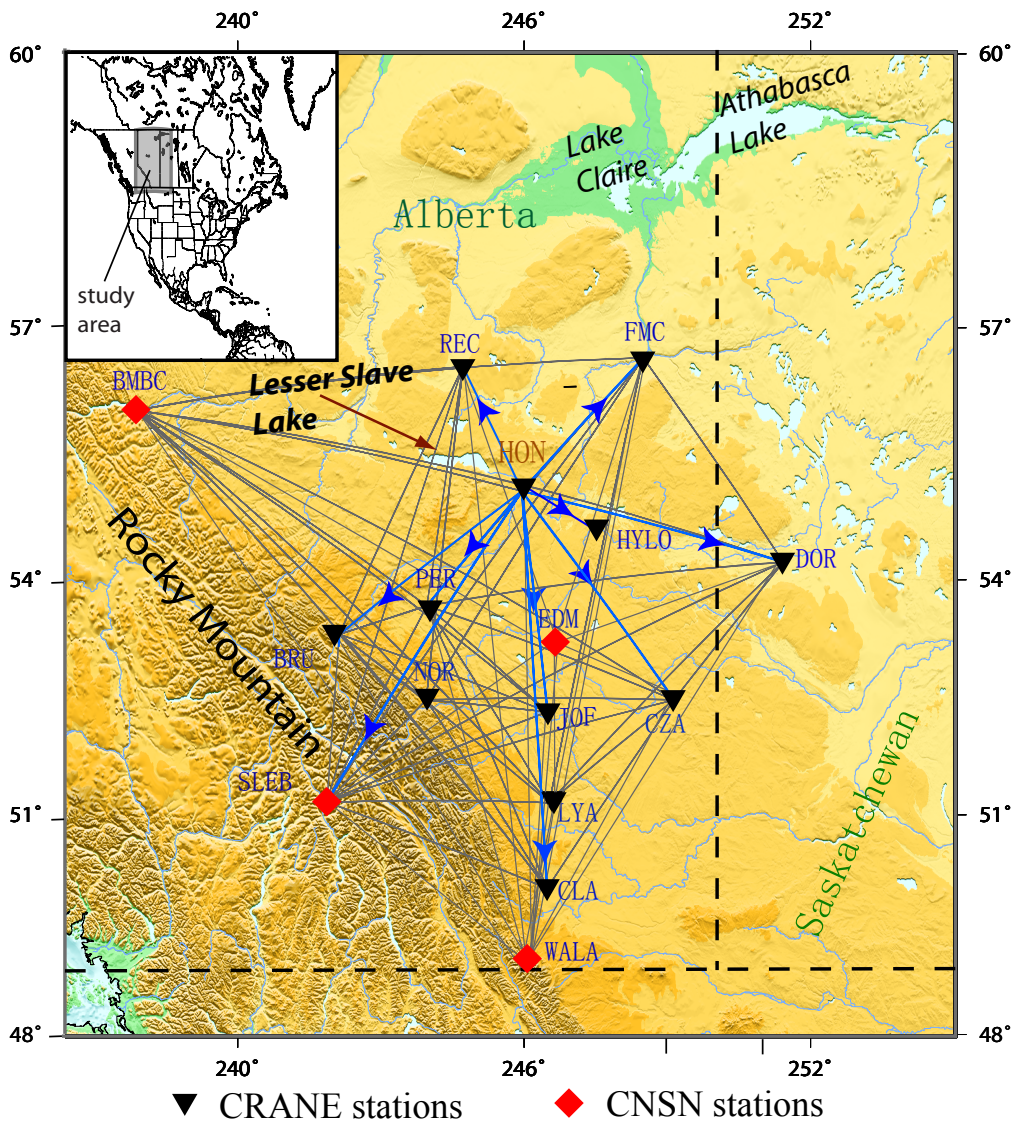


Figure 2.1: Distribution of stations from the Canadian Rockies and Alberta Network (CRANE, black triangles) and nearby Canadian National Seismographic Network (CNSN, red diamond). The background colors show the topography of the region. The thin gray lines connecting the stations indicate all station pairs analyzed by this study. The blue lines with arrows indicate the station pair and order (e.g., for A B, the arrow would point to B) used in the migration analysis. The map inset shows the position of the study region relative to North America. Records from HYLO (available since June, 2010) are used for waveform comparisons in Figures 2.3 and 2.9.

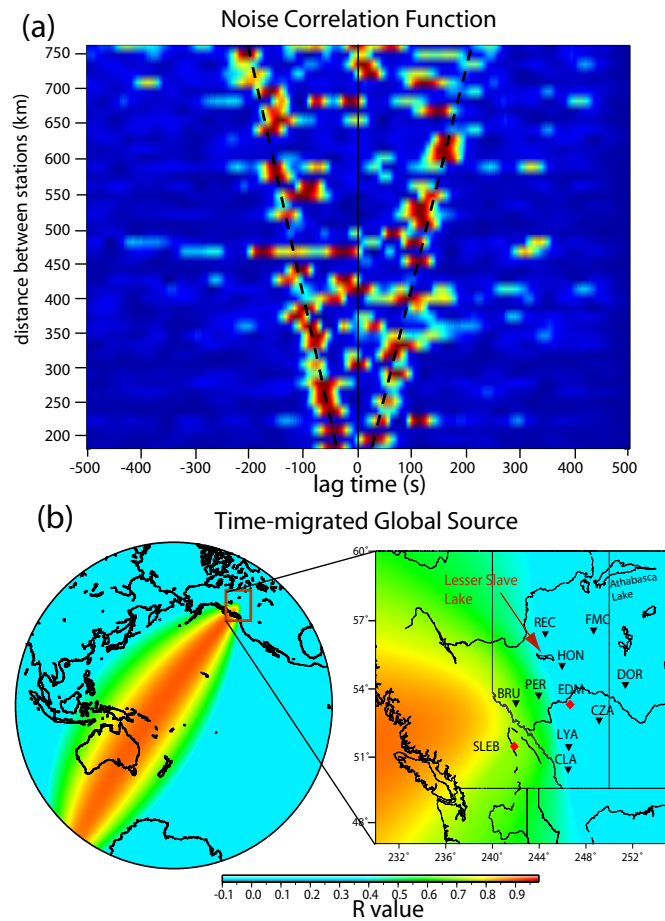


Figure 2.2: (a) Stacked cross-correlation functions (color-coded and slightly interpolated) for all station pairs denoted by gray lines in Figure 2.1. The dashed lines indicate the theoretical lag time based on a constant background velocity of 3 km/s. The lag time-distance relationship approximately follows two linear move-outs, but significant asymmetry is present on the individual correlation functions. By our sign convention, a negative lag on the SCCF of A x B implies that Rayleigh waves reaches station A first. (b) Source migration result using all station pairs connected by gray lines in Figure 2.1. The color scale shows the magnitude of values (maximum=1); a high value implies a strong probability that the true source is located at the center of the grid point under discussion. (c) A magnified view of the study region enclosed by the rectangular box in Figure 2.2(b). A dominant noise source is observed in the Pacific Ocean southwest of the station array.

and Tanimoto, 2007; Bensen et al., 2007; Koper et al., 2010] (Figure 2.2). By our sign convention, a negative lag from correlating stations A (from here on, anchor station) with B (denoted as) implies that noise energy consistently reaches station A prior to B. Symmetric SCCFs are generally interpreted as evidence of 'ambient' background noises [e.g., Shapiro et al., 2005; Bensen et al., 2007; Yang et al., 2007; Yao and van der Hilst, 2009], whereas asymmetry reflects biased source distributions relative to the receiver geometry [e.g., Paul et al., 2005; Gu et al., 2007; Yang et al., 2009; Brzak et al., 2009; Schimmel et al., 2011]. Despite a random selection of the anchor station in each station pair, a procedure that tends to enhance the symmetric appearance of SCCFs, the majority of the station pairs are highly asymmetric upon a trace-by-trace examination.

We utilize both time and waveform migration methods to determine the locations and strengths of potential noise sources. The study region (see 2.1) is partitioned into equal-area ($0.5 \times 0.5 \text{ deg}^2$) cells containing hypothetical noise sources. For each cell, the time-based migration approach defines a quantity based on the residual lag time between predicted and observed SCCF peaks,

$$R = 1 - \frac{1}{M * N} \sum_{i=1}^M \sum_{j=1}^N \left\{ \frac{(\Delta_i(x, y) - \Delta_j(x, y)) / v_g}{T_{ij}} - 1 \right\}^2 \quad (2.1)$$

where i and j are the number of stations ($= 1$ if the migration is performed on station pairs with the same anchor), and v_g is the average Rayleigh wave group velocity. Distances from a hypothetical source positioned at (x, y) to the i -th and j -th stations are represented by $\Delta_i(x, y)$ and $\Delta_j(x, y)$, respectively. Finally, T_{ij} (a scalar quantity) denotes the observed lag time of the noise correlation peak in the SCCF of the i -th and j -th stations. In essence, represents the normalized probability that a hypothetical source in cell coincides with the true source location. This method depends solely on the lag times of noise correlation peaks and will henceforth be referred to as 'time migration' [e.g., Shapiro et al., 2006]. .

To incorporate noise-correlation amplitude information and verify/refine the results of time migration, we define an independent migration time series where

$$A(t) = \frac{1}{M * N} \sum_{i=1}^M \sum_{j=1}^N X_{ij}(t + \frac{\Delta_i(x,y) - \Delta_j(x,y)}{v_g}) \quad (2.2)$$

The definitions of M , N , v_g and Δ in this formulation remain unchanged from Equation (1). For each cell position, the summation is now performed over time-shifted correlation stacks $X_{ij}(t)$ for a lag time. This formulation is similar to methods adopted by Rhie and Romanowicz [2006] and Brzak et al. [2009], as the time shift to each correlation stack is governed by the relative distances from a source to the i -th and j -th stations divided by the group velocity v_g . Finally, the maximum absolute amplitude of the stacked correlation function is used as an effective measure of the probability that the true noise source is located in a given cell.

The initial choice of v_g is based on the average shear velocity model of Gu et al. [2009] using teleseismic body wave data from the same array. The time migration of all station pairs for the entire frequency window shows large values west/southwest of the station formation (Figure 2.2b), highlighting the positive half of a great-circle path in the Pacific Ocean (Figure 2.2b). The global maximum is observed near Tonga-Fiji region, which is in the vicinity of a dominant global noise source in Yang and Ritzwoller [2008]. This potential source location is away from the nearest shoreline, thus favoring a mechanism involving nonlinear interactions of ocean waves [Longuet-Higgins, 1950; Haubrich and McCamy, 1969; Hasselmann, 1963; Hughes, 1976; Chevrot et al., 2007]. However, caution has to be exercised regarding this interpretation since only the source orientation could be determined with acceptable accuracy by the small-aperture receiver array. The insufficient data constraint on distance implies that potential noise sources originating from Hawaii [Schimell et al., 2011] and Pacific coastal ranges (e.g., near Vancouver island) cannot be excluded.

2.2 Local microseismic noise source

2.2.1 Travel Time Migration

The primary focus of this study is a second, local source within the WCSB. The lag times of correlation peaks at a number of stations are incompatible with those expected from noise sources in the Pacific Ocean. For example, the SCCF of (Figure 2.3a) is symmetric at low (0.01-0.06 Hz) and high (less than 0.19 Hz) frequencies, but intermediate frequencies are dominated by strong correlation peaks with large negative lag times. Based on the orientation of the migrated global source (Pacific Ocean southwest of station array, see Figure 2.2b), the absolute lag time of this asymmetric peak (greater than 100 s) well exceeds the time difference associated with paths connecting the global source with this station pair (less than 50 s). In other words, an additional noise source closer to HON than to DOR is required to explain the observed SCCF.

The need for a secondary noise source (see Figure 2.3a) is not coincidental. Similar signal characteristics are consistently observed on the SCCFs of station pairs anchored by HON (Figure 2.3b). The peaks of the SCCFs anchored by HON generally become more negative in lag time with increasing station separations, which imply that the energy from persistent ground movements reaches HON prior to other stations. To determine the regional source location and minimize the effect of the global source, we perform time migration based on all quality station pairs anchored by HON (see Figure 2.3b); the SCCF associated with HYLO is omitted due to insufficient data. The maximum value from time migration (Figure 2.4a) provides more quantitative support for a potential local noise source. The peak of the migration amplitude near HON nearly doubles the average values of the region north of the station array and quadruples those in southern Alberta. The uniqueness of this potential source location is evident from a comparison of three hypotheti-

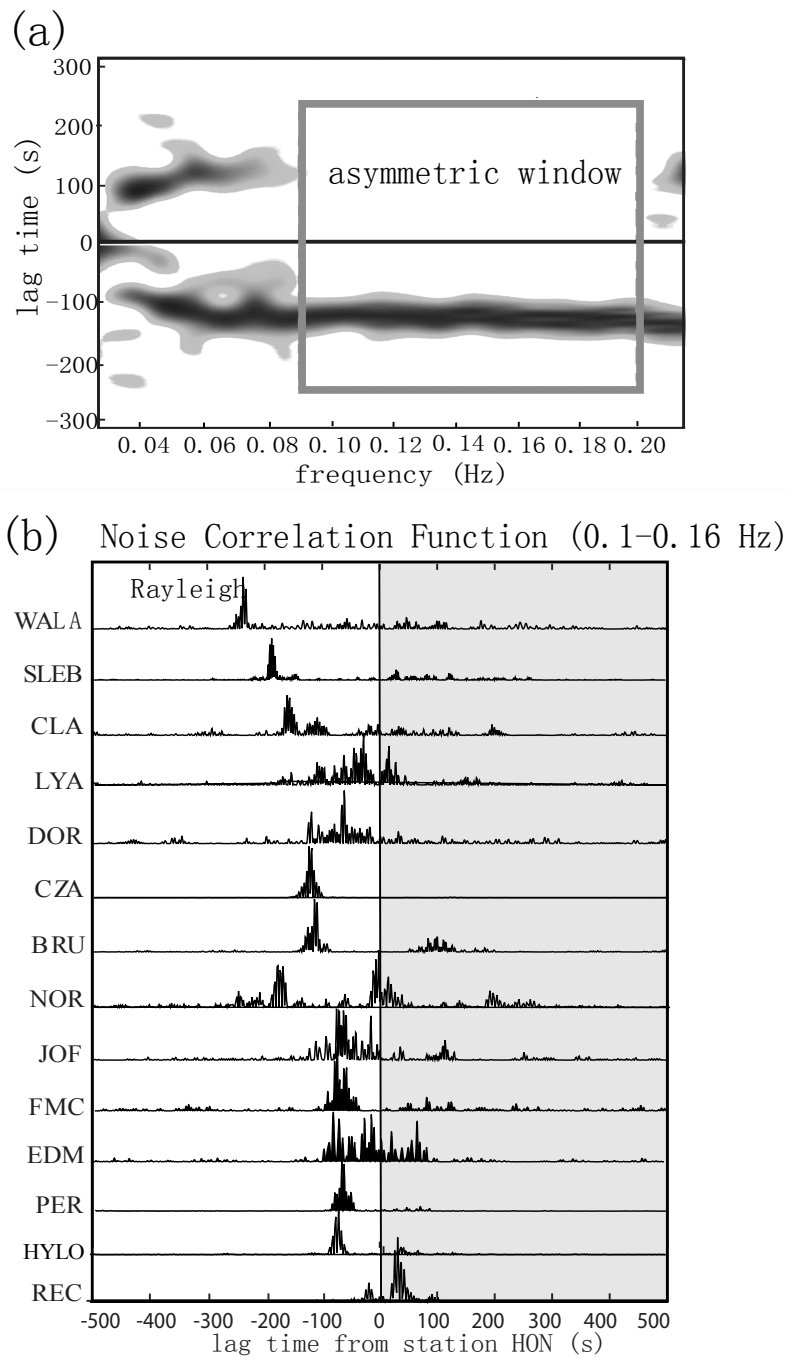


Figure 2.3: (a) Vertical component cross-correlation of station HON (anchor) and DOR for a cutoff frequency range of 0.01-0.2 Hz. The SCCF is computed by a series of narrow band-pass filters within the frequency range of interest. The move-out curve is symmetrical at both low and high frequencies but shows strong asymmetry in the range of 0.08-0.16 Hz. (b) Normalized absolute values of SCCFs of station pairs anchored by HON. The shaded region highlights the positive lag times, which roughly follow a semi-linear relationship. With the exception of HYLO, all SCCFs are used in regional source migrations.

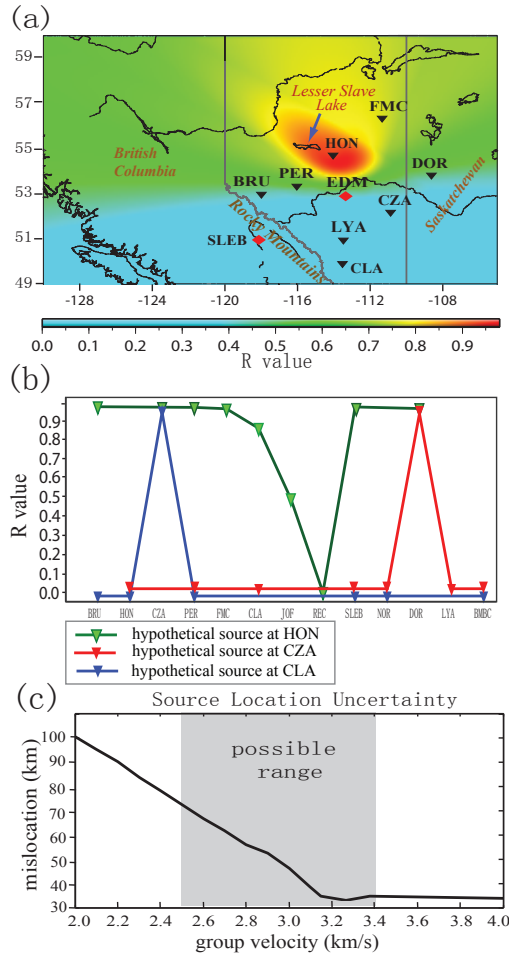


Figure 2.4: (a) Time-migrated values of the study region. A cell with a large value implies a strong possibility of containing the true noise source. The maximum value is observed near LSL, though the precision of the noise source location is limited by station density. (b) values of station pairs based on a background Rayleigh wave group velocity of 3.0 km/s and hypothetical noise sources at the station locations of HON (green), CZA (red) and CLA (blue), respectively. As a simple example, for a hypothetical source at CZA (also the location of the anchor station) and station NOR (plotted as a red inverted triangle) is computed based on Equation (1) while assuming 1) , and 2) is the observed lag time of the SCCF between CZA (anchor station and hypothetical source) and NOR. The inverted triangles indicate station pairs with robust noise correlation peaks and stations that resulted in poor correlations with the majority of the three anchors (e.g., WALA) are omitted. c) Migration results based on background velocities ranging from 2.0 to 4.0 km/s. The vertical axis shows the distance between the resulting noise source location and reference point in east basin of LSL. The shaded region marks the range of realistic background velocities ranging from 2.5 to 3.4 km/s [Gu et al., 2011].

cal source locations (Figure 2.4b). In this hypothesis test, values are computed for station pairs (i.e., in Equation (1)), assuming a 3 km/s background velocity and a hypothetical source at the anchor station (HON, CZA and CLA are used as anchors for this test). The value at a given station is inversely proportional to the time difference between the predicted and observed lag times, and the average associated with a hypothetical source at HON is 0.6-0.8 higher than that of the two remaining source locations (see Figure 2.4b). In fact, the only large values from hypothetical sources away from HON (e.g., CZA in blue, Figure 2.4b) are results of autocorrelation (defaulted to 1) (see Figure 2.4b).

The main source of uncertainty is the selected Rayleigh wave group velocity during travel time migration. The subjective choice of a constant average velocity for the study region can introduce errors to the source location due to 1) crust and mantle 3D heterogeneities and 2) difficulties in accommodating dispersive surface waves with a single 1D velocity. Heterogeneous path effects are clearly demonstrated by an anomalously delayed peak in the SCCF of (see Figure 2.3b), where shear wave velocity is ~10-15% slower than the regional average based on a preliminary analysis of the same data set [Gu et al., 2011]. Unfortunately, reliable crust and mantle velocity models of WCSB remain a work-in-progress, largely owing to the lack of receivers prior to the establishment of CRANE. We repeat the experiment shown in Figure 2.3a with a wide range of migration velocities to assess the source location dependency on velocity. Figure 2.4c shows the distances between the resulting source locations and a reference point in the eastern bay of LSL, a potential source location. Mislocations range from 30 to 100 km for all selected migration velocities. Within a realistic group velocity range of 2.5-3.4 km/s [Gu et al., 2011], mislocations decrease with increasing velocities but stabilize at large values. The latter observation can be attributed to decreased imaging resolution when the Rayleigh wave travel time differences between station pairs become neg-

ligible under unrealistically large wave speeds. Considering the limited number of stations, coarse migration grid size and errors associated with 1D approximation, a realistic estimate of location uncertainty is 60-100 km from the reference position.

Location uncertainty is negatively impacted by the SCCFs associated with BMBC and REC. First, the results of BMBC are inconsistent with signatures from all three hypothetical sources (Figure 2.4b), which may be caused by 1) low signal qualities at large distances from the optimal location of the regional source, and/or 2) competing source effects from the Pacific Ocean. Low data quality also affects REC, as the SCCFs from four adjacent station pairs anchored by REC (NOR, PER, EDM, BRU) show little, if any, indications of correlated background noise (Figure 2.5). Station REC was extracted prematurely within a year of operation due to severe water damages to the instrument vault. While the source of flooding was later determined to be a catastrophic failure involving local frost heaves, the impact of vault condition deterioration on the data recorded prior to the failure remains uncertain. Still, the robust signal from the SCCF of is unlikely to be instrument related (see Figure 2.5). The sign of the lag time indicates that noise energy reaches REC first, which requires a short path to REC and/or a slow path to HON. Both conditions can be satisfied if the true noise source resides within the west bay of LSL: in addition to a slightly greater distance to HON than to REC, energy from this potential source needs to travel the full length of LSL across a seismically slow layer containing water, ice (if in winter) and thick lake sediments. Validation of this hypothesis would, however, require further improvements to the existing source location.

2.2.2 Waveform Migration

The addition of waveform information based on Equation (2.2) provides further evidence of a persistent microseismic source near LSL. Based on station pairs anchored by HON and an average group velocity of 3.0 km/s [Gu et al., 2011], the

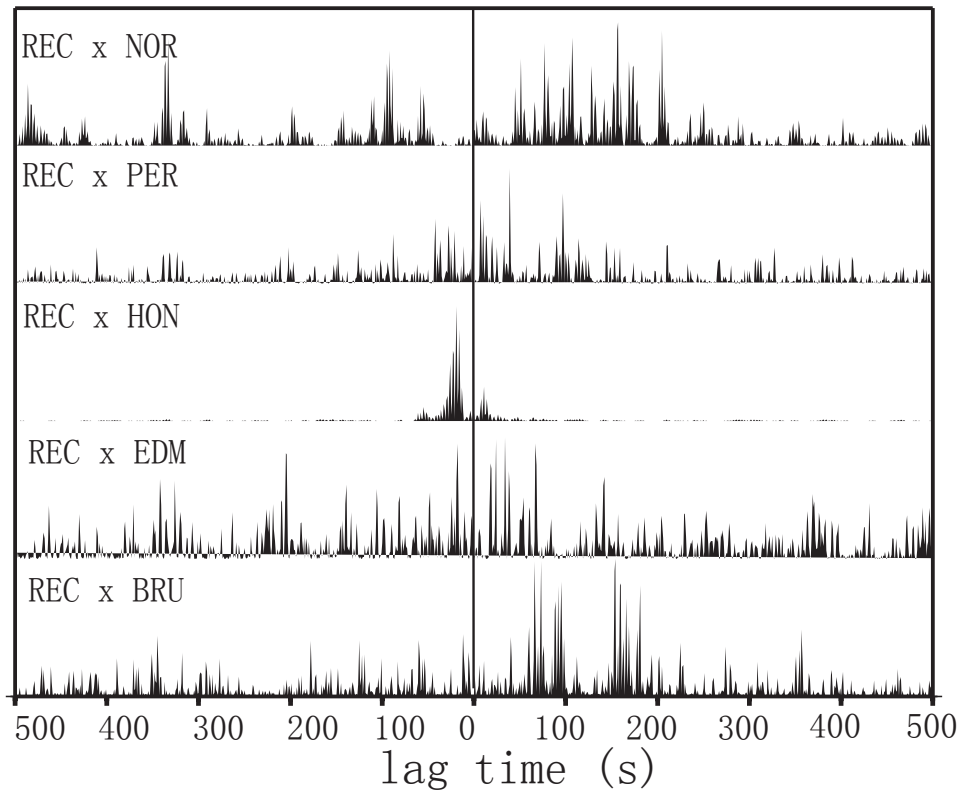


Figure 2.5: Sample noise correlation stacks computed from REC (anchor) and five nearby stations. Low signal-to-noise ratios are observed on four stations, which reflects data quality issues. The final correlation pair provides additional information on the location of the potential regional noise source (see main text).

result of waveform migration shows an elongated high probability zone in the western part of the station array (Figure 2.6). A local amplitude maximum is observed in northern-central LSL, which is approximately 80-100 km northwest of the regional maximum from the time migration (see Figure 2.4a) and the amplitude nearly doubles those in southeastern Alberta. The location and strength of the noise source are moderately dependent on the 1D migration velocity (Figure 2.7). For instance, the choices of $v_g = 2.5$ km/s and $v_g = 2.9$ km/s result in strong migration amplitudes around LSL, whereas $v_g = 3.1$ km/s tends to shift the local maximum to the southwest by 100-120 km. A rough estimate of the location uncertainty is 80-120 km, with the respective uncertainties of ~ 100 km and ~ 50 km in longitude and latitude (see Figure 2.7).

Large migration amplitudes near the western boundary of the study region, especially for cases where $v_g = 2.9$ km/s, underscore a key difference between the outcomes of time and waveform migrations. For time migration, the influence of global sources is minimized by restricting the analysis to the subset of station pairs anchored by HON (see Figure 2.4a). This approach is not nearly as effective in waveform migration due to the complexity and sensitivity of correlation amplitudes. The anomalously high migration amplitudes near the western boundary of the study region show no visible signs of decay. In view of the low sensitivity of SCCFs to distance, this observation could be caused by a remote noise source outside of the study region. The projected orientation of this source (west) differ with that suggested by time migration approach (southwest, see Figure 2.2b), thus raising questions about the existence of a second global source away from the study region. In the case of waveform migration, the Pacific coast of Canada is an appealing landward entry point of the source energy resulting from either coastal impact or pelagic sources (e.g., Schulte-Pelkum et al., 2004; Shapiro et al., 2005; Sabra et al., 2005; Gerstoft and Tanimoto, 2007; Gu et al., 2007; Chevrot et al., 2007;

Waveform Migration (0.08 – 0.16 Hz)

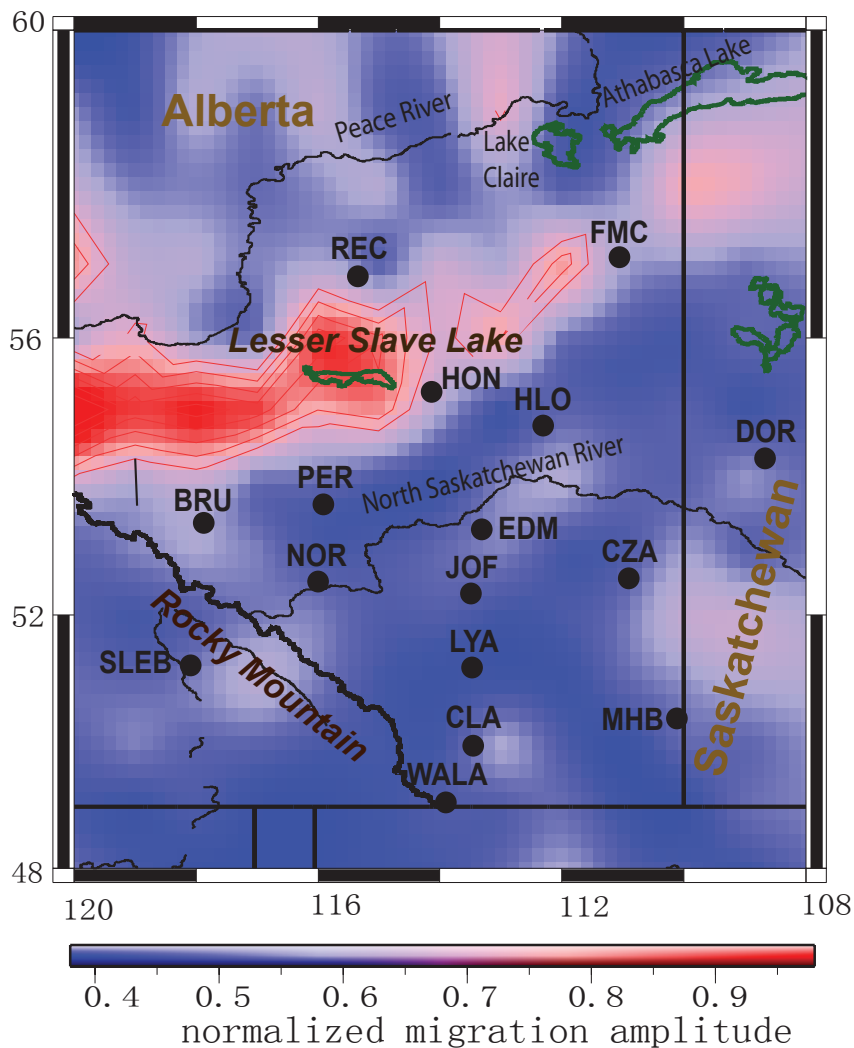


Figure 2.6: Result of waveform migration based on Equation (2). The individual SCCFs were filtered between 0.08 Hz and 0.16 Hz prior to migration, and the background Rayleigh wave group velocity was set at 3.0 km/s. Large migration amplitudes are observed near LSL, potentially extending to the western boundary of our study region.

Effect of Migration Velocity

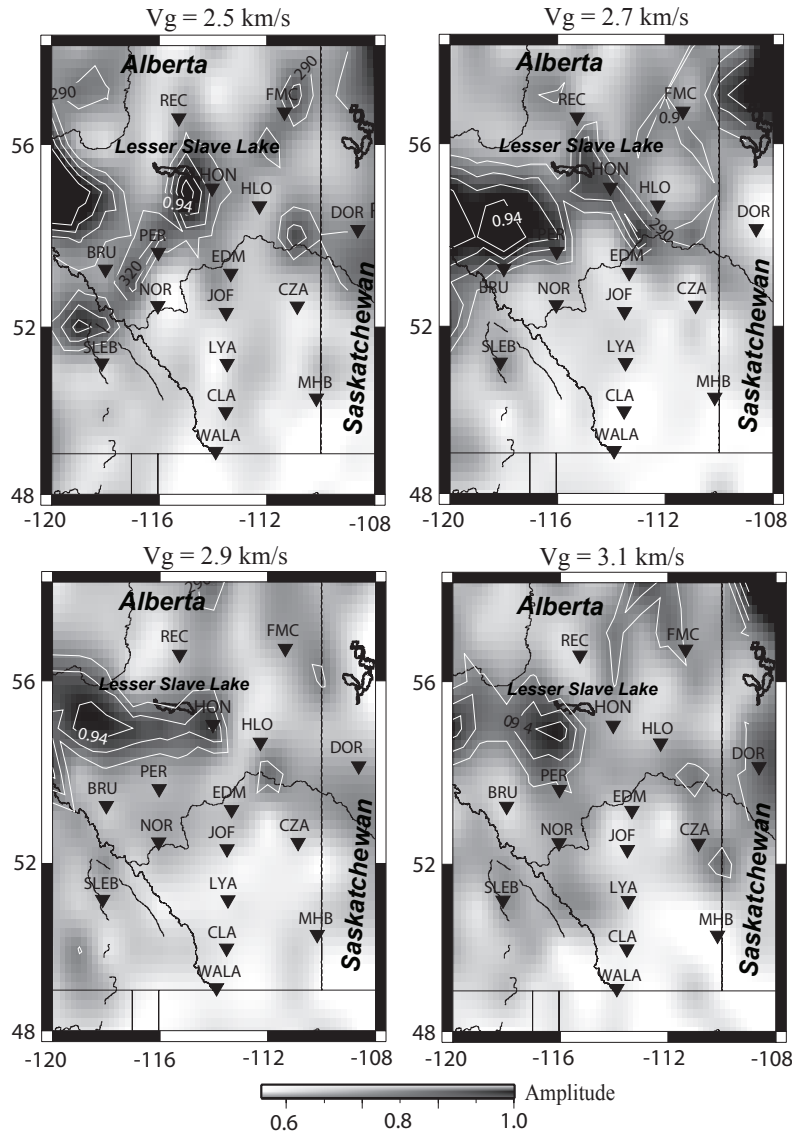


Figure 2.7: Waveform migration results from four different Rayleigh wave group velocities. A local maximum is consistently observed in the vicinity of LSL. The estimated location uncertainty based on the movement of the source is 100-120 km. Effects of background velocity on source location are underscored by the large migration amplitudes near the northwestern boundary of the study region when falls below 2.7 km/s.

Yang and Ritzwoller, 2008; Brzak et al., 2009; Ardhuin et al. 2011; Shimmel et al., 2011). The strengths of potential global noise sources from both migration approaches are susceptible to influences from the shape and topography of associated coastlines, from atmospheric pressure and ocean swells, as well as from the ground attenuation of the land portion of great-circle paths connecting noise sources and receivers.

2.2.3 Frequency Dependence of Noise Energy

Seismic background noise has been recorded at frequencies ranging from a few millihertz, which is characteristic of continuous background free oscillations known as 'hums of the Earth' [Suda et al., 1998; Tanimoto et al., 1998; Rhie and Romanowicz, 2006; Webb, 2007], to tens of Hertz. Their origins remain inconclusive [Webb, 2007], though recent observations have suggested atmosphere/ocean/seafloor coupling as a major contributing factor at all frequencies [Stehly et al., 2006; Rhie and Romanowicz, 2006; Shapiro et al., 2006; Yang and Ritzwoller, 2008; Kedar et al., 2008]. The frequency band of interest in this study is (0.01-0.2 Hz), a range highlighted by energetic spectral signals at 0.05-0.08 Hz (primary microseisms) and 0.1-0.3 Hz (secondary microseisms) [Longuet-Higgins, 1950; Gutenberg, 1951; Hasselmann, 1963; Haubrick and McCamy, 1969; Hughes, 1976]. The asymmetric dispersion relation exhibited by the SCCF of (see Figure 2.3a) is, to first order, consistent with the spectral characteristics of ocean microseisms.

In order to systematically quantify the frequency dependence of asymmetric SCCFs and noise source location(s) [e.g., Frank et al., 2009], we re-filter the broadband datasets and repeat waveform migration over four narrow frequency bands while assuming a constant migration velocity of 3.0 km/s (Figure 2.8). At a center frequency of 0.34 Hz, an isolated migration peak is detected at 80 km distance from the western part of LSL. The strength and dimension of this high-probability

Frequency Test

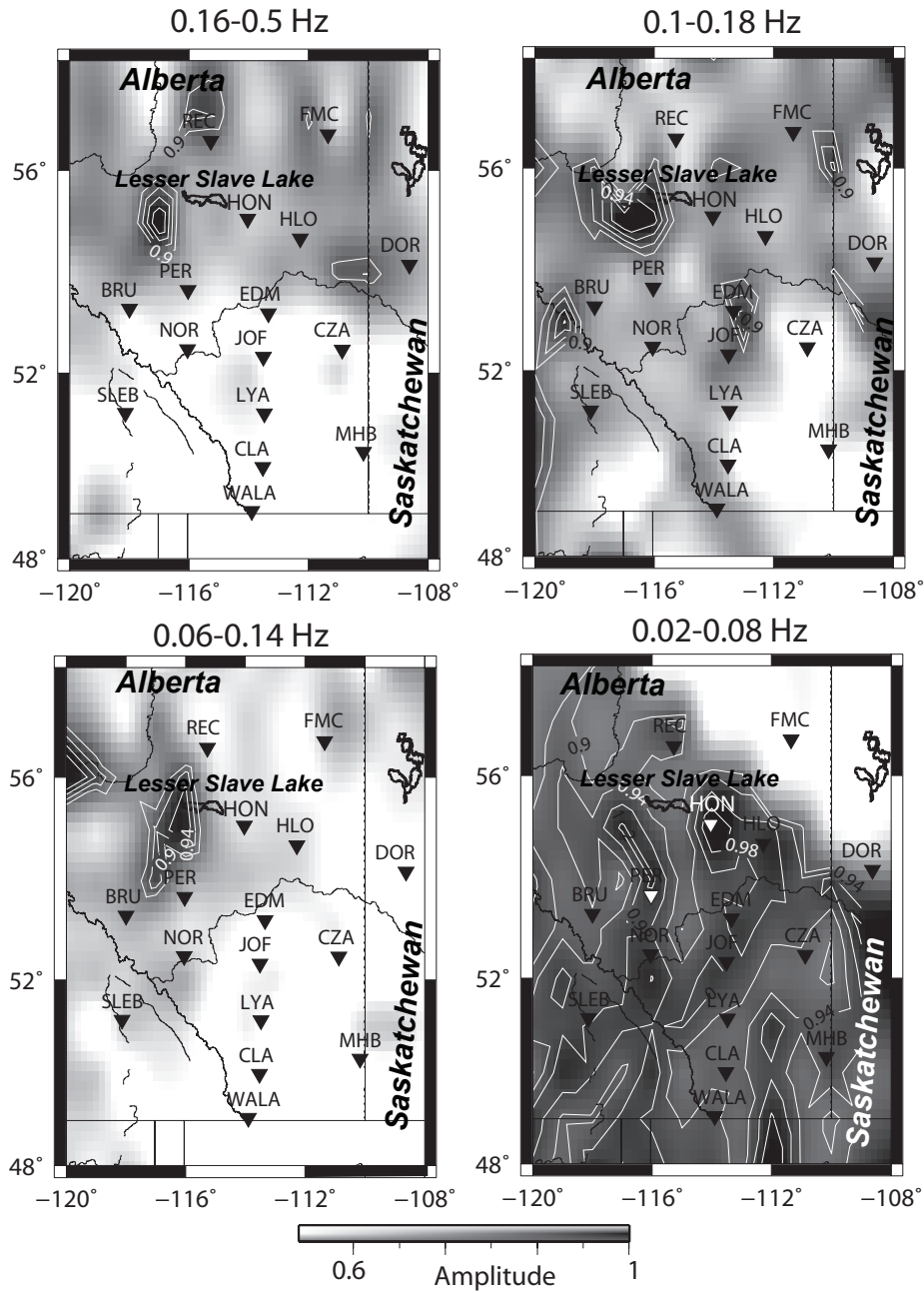


Figure 2.8: Waveform migration results from four slightly overlapping frequency bands. Strong migration amplitudes are observed near the west bay of LSL, particularly in the typical frequency range of ocean microseisms (0.06-0.18 Hz). The effect of the local noise source is minimal at longer periods (0.02-0.08 Hz, bottom right) as noise correlation functions become increasingly symmetric.

zone increase substantially in the secondary microseism range (0.1-0.18 Hz), and the center of the migration peak is observed less than 50 km away from LSL (see Figure 2.8). The strength of the same migration peak remains significant at primary microseism frequencies (0.06-0.14 Hz), though the global maximum amplitude shifts to the northwestern part of the study region at 56-deg latitude. Despite these differences, however, the main observations from all three aforementioned frequency ranges are consistent and suggest a common local source with overlapping frequencies to those of ocean microseisms. The migration results severely degrade at the center frequency of 0.05 Hz (see Figure 2.8) where a local maximum near the southeastern part of LSL is only marginally above the regional average. This characteristic change from other frequencies can be attributed to increasingly symmetric correlation functions, as demonstrated in Figure 2.3a, at frequencies below ~ 0.06 Hz.

2.3 Discussion

Asymmetric SCCFs have been widely observed [e.g., Schulte-Pelkum et al., 2004; Shapiro et al., 2005; Sabra et al., 2005; Gerstoft and Tanimoto, 2007; Gu et al., 2007; Yang and Ritzwoller, 2008; Ardhuin et al., 2011] and numerically simulated [Stehly, 2006; Chevrot et al., 2007; Kedar et al., 2008; Brzak et al., 2009; Ardhuin et al., 2011; Shimmel et al., 2011] in recent years. In most cases, amplitude symmetry can be associated with preferred directionality of the noise field surrounding stations [Frank et al., 2009]. This study is predicated on this premise and, despite notable differences in the outcomes, our travel-time and waveform migrations of SCCFs from a regional broadband array jointly suggest a local noise source in the vicinity of LSL. A simple demonstration of the noise source is presented in Figure 2.9. In this example, four station pairs anchored by HON form two azimuth

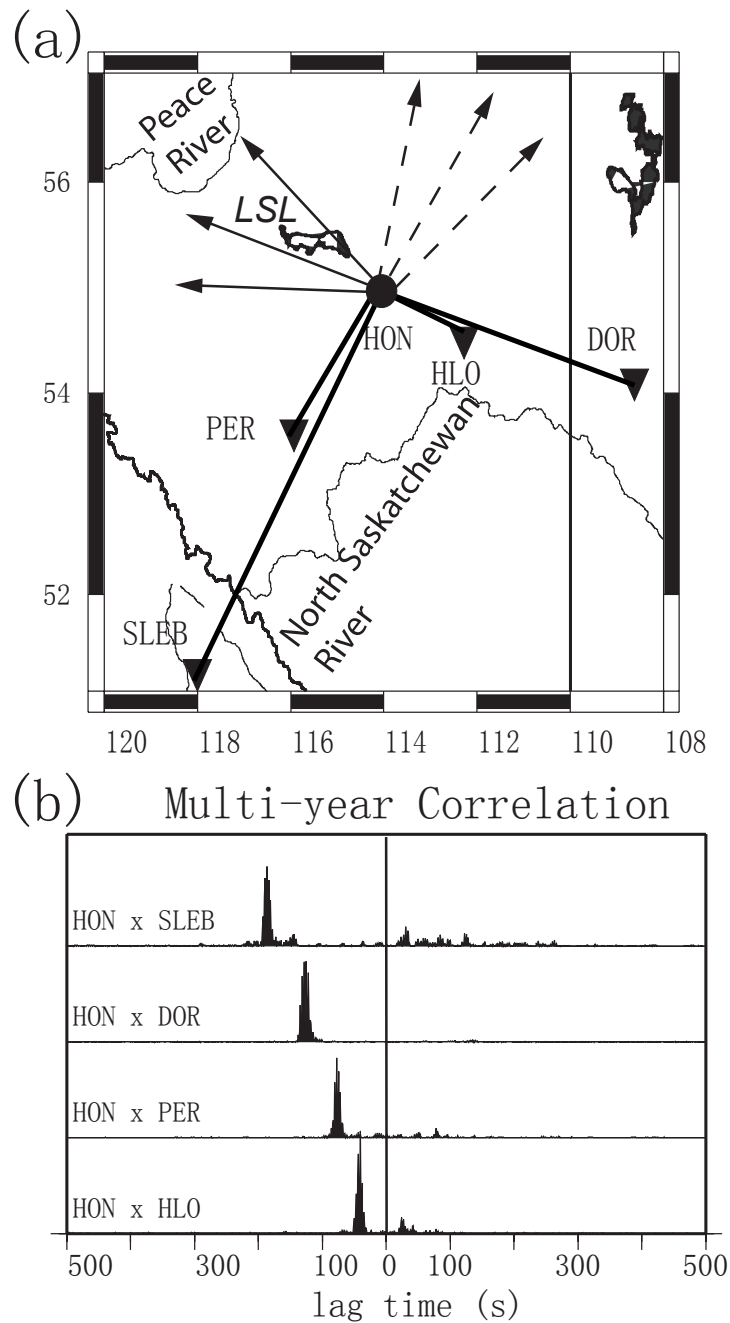


Figure 2.9: (a) Geographical location and path coverage provided by HON and four nearby stations. The solid and dotted lines with arrows indicate the expected source orientations based on the signs (all negative) and lag times of the SCCF maxima. (b) SCCFs computed for station pairs shown in Figure 9a based on recordings from 2007 to 2010. The high quality SCCFs show pronounced asymmetric correlation peaks with negative signs. In view of the unique geometries of these stations, a single local noise source must be present in the vicinity, preferably in the northwest, of HON.

bins separated by 90 deg angle (Figure 2.9a). The high quality SCCFs computed from four years of continuous recordings (2007-2010) show pronounced asymmetric correlation peaks with negative signs, which imply 1) noise energy from each potential source reaches HON prior to other stations, and 2) the additional distances traveled by the noise energy after reaching HON are comparable to station separations. Mechanisms involving two independent global/remote sources [e.g., Chevrot et al., 2007; Yang and Ritzwoller, 2008; Pawlak et al., 2011] can satisfy the timing requirements from the SCCFs, but multiple sources oriented nearly perpendicularly to each other should also produce distinctive correlation peaks on each SCCF. The latter assumption is clearly at odds with the vast majority of SCCFs shown in Figure 2.9. As the only viable alternative, a single source is required in the vicinity (preferably to the northwest) of HON based on the path geometries.

A broad range of environmental factors including oil/gas surveys, natural ground motion and water flow could contribute to the observed microseisms near HON/LSL. We hereby assess the importance of each factor based on existing knowledge about the potential source region and the characteristics of the observed SCCFs. First, the frequency of ground motion caused by active oil/gas surveys or logging activities are generally greater than 5 Hz [Yilmaz, 2001], which is significantly higher than the observed asymmetrical frequency range (0.08-0.15 Hz). More importantly, based on the published report of industrial activity by Alberta Energy in 2009, major projects have been ongoing at oil/gas hotspots such as Fort MacMurray, Cold Lake and Peace River. Should exploration activities be responsible for source migration amplitude and SCCF asymmetry, the expected severity of ground movements in the vicinity of these 'hotspots' would be comparable to, if not greater than, that near LSL. Unfortunately, this assumption is not supported by the observed SCCFs and source locations inferred from figures 2.4 to 2.9.

Questions of uniqueness are equally valid for known geological processes such

earthquakes or continuous creep [Brooker and Peck, 1993; Mansour, 2009] in response to stress accumulation and release in the WCSB. Earthquakes up to $M_w=5.5$ have previously been recorded in Alberta according to Earthquake Canada (see Data and Resources Section), though known activities in the vicinity of HON has been limited to date. A recent study based on CRANE and nearby permanent stations [Stern and Gu, 2011] shows that most of the recent regional microseismicities are concentrated along the Rocky Mountain foothills and southernmost Alberta. Other detectible events such as mining blasts (e.g., Wabamum Lake, [Stern and Gu, 2011]) and landslides (e.g., Turtle Mountain [Brooker and Peck, 1993; Friedmann et al., 2003; Pedrazzini et al., 2008] and Peace River [Cruden et al., 1990; Davis et al., 2005; Morgan et al., 2008]) are simply too far from the potential noise source region to be considered major contributing factors. Still, in the absence of strong moment releases in the potential source region, the seismic potential and characteristic frequencies of continuous stress releases interweaving with the effect of ocean microseisms [Frank et al., 2009] remain plausible in the vicinity of LSL.

The SCCF peak frequencies generally favor water as a key ingredient in the generation of dominant seismic noise. While the WCSB is devoid of oceans and seas, LSL and channels of the Athabasca River are both potential sources of microseisms. A comparison of independent SCCFs from the winter (Dec 2007-March 2008) and summer (May 2008-Oct 2008) months (Figure 2.10a) offers additional insights into the timing and mechanics of the noise source. The winter SCCFs are highly asymmetrical and well correlated with the observed asymmetry on the annual SCCFs. The summer SCCFs are, in comparison, significantly more symmetric (see Figure 2.10a). Since Athabasca River is fully frozen during the winter months, the contribution of discharge from the Athabasca River to the observed SCCF asymmetry would be minimal.

The complex hydrodynamics associated with LSL are a potential cause of the

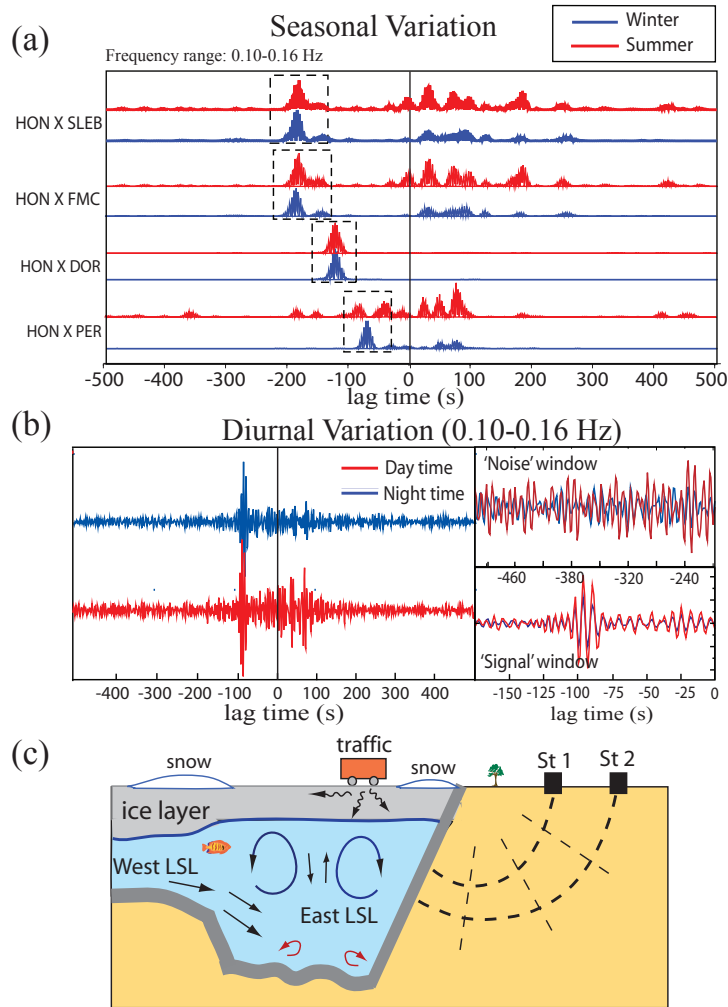


Figure 2.10: (a) Seasonal variations of the SCCFs in 2008. This one-year data set is divided into two time periods (see main text) and the same correlation analysis is applied to each subset. In comparison with the summer months, the resulting SCCFs show much greater asymmetry during the winter of 2008. (b) Sample diurnal variations (for station pair HON and PER) during the winter months. The SCCFs are consistent between night and day, which suggest a common origin or mechanism. The 'signal' part of the SCCFs (-150 s to 0 s, bottom right) are more consistent than the 'noise' part of the SCCFs (-500 s to -200 s, top right) for the daily analysis. The amplitudes have been self-normalized for both time windows. (c) A schematic diagram illustrating the potential origins of microseismic noise. Mixing and resonance, as well as human activities and environmental processes, may be responsible for the asymmetrical SCCFs.

observed microseismic signals during winters. While the discussions of limnology and oceanography have been interleaving, the size, depth, stratification, surface movement and bottom topography are substantially different between lakes and oceans [Kenney, 1991, 1996; Malm, 1999]. Both human and environmental factors may be important in generating lake microseisms at LSL. As the largest lake fully contained in Alberta and one of Canada's most popular ice fishing sites, constant traffic on the frozen lake via various ice roads can cause significant vibrations on the lake ice layer. Vertical movements can easily be felt by a person standing on the ice surface and are capable of inducing turbulence beneath ice cap. Increased industrial traffic surrounding the lake during the winter months (e.g., freighter trains and lake-side traffic) may also contribute to the episodic pressure changes within the ice-covered lake. However, the limited diurnal variation of the noise signals during the winter of 2008 (Figure 2.10b) places rather restrictive timing constraints on these activities.

Natural causes of horizontal and/or vertical flow [Wuest and Lorke, 2003] beneath the 1-2 m thick ice surface are a plausible cause of lake microseisms (Figure 2.10c). Significant under-ice circulation have been previously reported in Tub lake [Colman and Armstrong, 1983], Wupaw Bay [Kenney, 1991, 1996], Harmon lake [Rogers and Lawrence, 1995], Lake Baikal [Kelley, 1997], Vendyurskoe Lake [Malm, 1999; Petrov et al., 2007] and, in a slightly different setting, Hungry Horse reservoir [O'Connell, 2007]. Based on information provided by a wide range of hydraulic measures, the strength of under-ice circulation of up to tens of mm/s are predicated on key attributes such as snow coverage, sediment heat flow [Rogers et al., 1995; Kelley, 1997], ice- and water-layer thicknesses, and bottom topography [e.g., Polzin et al., 1997]. Substantial lateral variations of these parameters are expected over a large lake, especially for LSL where the average depths of two approximately equal-area bays (connected by a narrow channel) differ by sev-

eral meters. The substantial lake-bottom topography could facilitate turbulence and mixing, especially in the western bay, and cyroseisms (or frost quakes) due to extreme winter temperature variations are also conducive to the generation of internal waves [e.g., Polzin et al., 1997; Malm, 1999]. Once a source of excitation is present, LSL can act as a filter such that only certain modal frequencies (e.g., 0.06-0.2 Hz) are retained, resonated and potentially amplified within the bounded system of ice, water and sediment (see Figure 2.10c).

Wind may also contribute to noise generation and the observed seasonal variations. According to Canadian Wind Energy Atlas (see Data and Resources Section), the mean wind energy near LSL is 700 W/m² and 300 W/m² during the winter and summer months of 2010, respectively (Figure 2.11). Outside the foothills of the Rocky Mountains — the regional maximum due to pressure variations associated with extreme topographic relief, these levels are substantially larger than those of the surrounding regions including major water bodies 6-8 times larger in surface area (e.g., the Greater Slave Lake and Athabasca Lake) (see Figure 2.11). Strong wind and ice storms would undoubtedly enhance ground motion in and around the lake, though it remains questionable whether the reported wind energy levels are sufficient to cause sustained microseismic signals near LSL.

Another key contributing factor to the observed seasonal variations is ground attenuation [e.g., Arduin et al., 2011; Schimmel et al., 2011]. According to a recent study by Schimmel et al. [2011], low attenuation is largely responsible for strong SCCFs sampling old continents and isolated ocean islands (e.g., Hawaii). For the case of LSL, the amplitude and asymmetry of the SCCFs of the winter months could benefit from a weakly attenuating medium due to the solidification of 'muskegs' (or, grassy bogs).

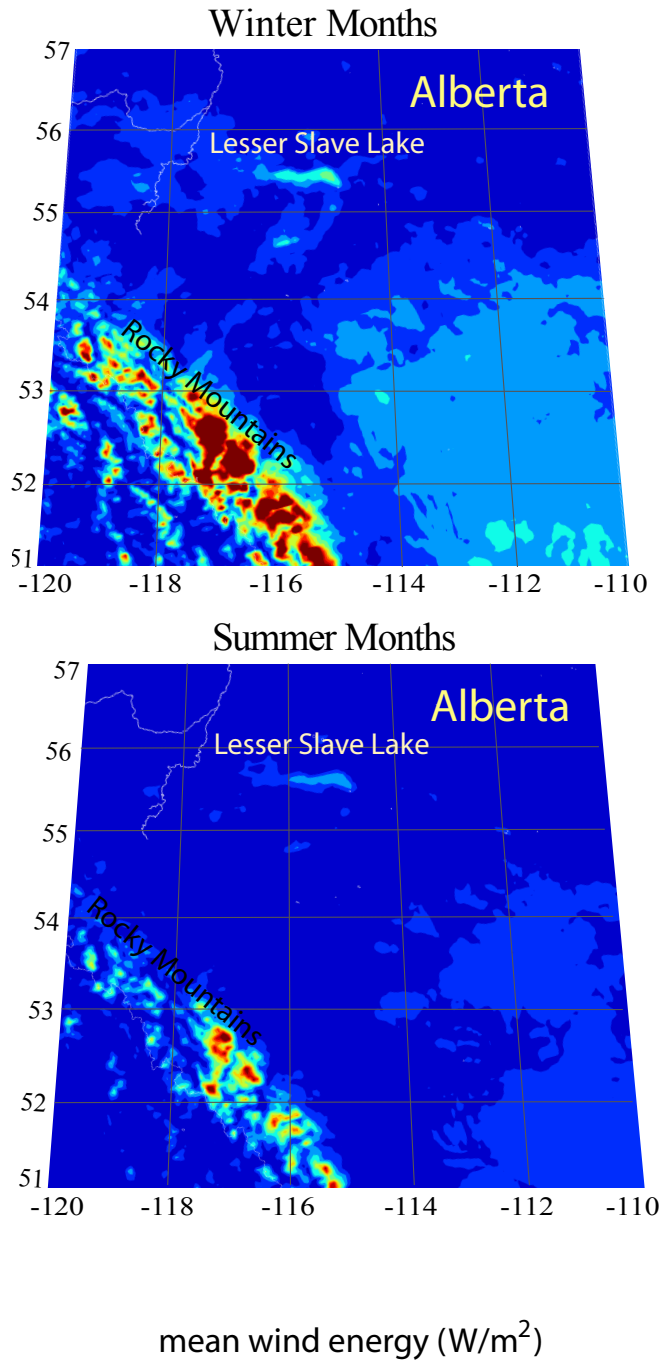


Figure 2.11: Mean wind energy during the winter (top panel) and summer (bottom panel) months of 2010 (see Data and Resources Section). Extreme values are observed along the Rocky Mountain front due to extreme topographic reliefs. Strong wind energy in the vicinity of LSL, which far exceeds those near water bodies of much greater sizes (e.g., Great Slave Lake, Athabasca Lake), could play a possible role in the generation of persistent local noise sources.

2.4 Conclusion

Based on asymmetrical seismic noise records from a local broadband array and multiple source migration methods, we are able to determine a persistent local noise source beneath the relatively 'quiet' southern-central Alberta region. The peak of the effective probability function varies with assumed migration velocity and wave frequency, underscoring an estimated location uncertainty of ~100-150 km around LSL. The frequency of the asymmetric correlation window is consistent with those of global ocean microseisms.

The origin of this noise source remains inconclusive, though it is clear that the energy associated with the excitation can reach broadband seismic receivers several hundred kilometers away. We highlight lake microseism as an intriguing possibility after reviewing various known mechanisms for regional noise generation. Our hypothesis is aided by the absence of known microseismic sources/mechanisms in the region and the spectral content of the asymmetric SCCFs, while limited observational and theoretical support, moderate source location uncertainty and interfering ocean microseism are legitimate concerns. Improved source location and characterization [e.g., Schimmel et al., 2011], as well as a greater understanding of lake hydrodynamics, will be necessary to reliably determine the nature of the observed microseisms in southern-central Alberta.

Chapter 3

Noise correlation tomography of the southern Western Canada Sedimentary Basin

3.1 Tectonic Setting

The age of Alberta's crystalline basement ranges from 1.7 to 3.2 Ga. The Archean and early Proterozoic basement domains in this region were more severely deformed and metamorphosed at 1.8-1.9 Ga than the adjacent Superior, Wyoming, Slave and Nain provinces [Hoffman, 1988]. Due to extensive sedimentation during the Phanerozoic era, the construction of regional tectonic models [Burwash and Krupička, 1969, 1970; Burwash and Culbert, 1976; Ross *et al.*, 1991; Hoffman, 1988; Villeneuve *et al.*, 1993] mainly relied on aeromagnetic/potential field data, isotope age determination on drill core samples and the extrapolation of tectonic elements from the exposed part of the Canadian shield [Hoffman, 1988; Villeneuve *et al.*, 1993]. Over twenty juxtaposed domains [Ross *et al.*, 1991] were identified in an oddly shaped region bounded by Great Slave Lake shear zone (GSLSZ), Snowbird Tectonic Zone (STZ) and Vulcan structure (VS), three major tectonic discontinuities [Eaton *et al.*, 1999b; Ross *et al.*, 2000; Clowes *et al.*, 2002; Berman *et al.*, 2007] that play key roles in defining and interpreting smaller tectonic domains. In particular, STZ divides the Archean Hinterland of Trans-Hudson Orogen and has

been widely recognized as a steep lateral gradient in gravity and magnetic field into Hearne and Rae Provinces [Hoffman, 1988; Ross *et al.*, 2000; Jones, 2002].

North of STZ, Buffalo Head Terrane (BHT), Taltson Magmatic Zone (TMZ) and Rae Province [Ross *et al.*, 1991; Villeneuve *et al.*, 1993] are three distinct tectonic domains recognizable from predominantly north-trending, convex-westward aeromagnetic signatures [Ross *et al.*, 1991; Hammer *et al.*, 1995; Ross and Eaton, 2002]. BHT mainly consists of metaplutonic and subordinate felsic metavolcanic rocks with ages of 2.0-2.32 Ga [Ross *et al.*, 1991; Villeneuve *et al.*, 1993]. The scattered aeromagnetic patterns in this microcontinent are compelling evidence for the complex assemblage of crustal fragments. East of BHT, the convergence of Slave and Rae provinces during Paleoproterozoic era [Theriault and Ross, 1990; McNicoll *et al.*, 2000] gave rise to the Taltson-Thelon Orogen, a north-trending magmatic belt comprised mainly of felsic metaplutonic and metasedimentary rocks. The roughly 3000-km long Taltson-Thelon Orogen cuts across multiple older domains and eventually terminates along STZ in central Alberta. The southernmost section of this orogen is generally referred to as TMZ, a 300-km long section containing both Archean and Paleoproterozoic metaplutonic gneisses but is distinctively younger than BHT [McNicoll *et al.*, 2000; McDonough *et al.*, 2000].

The tectonic domain resides immediately to the west of BHT is Chinchaga domain, an aeromagnetic low with a concordant shape. Drill cores from this region indicate extensive metaplutonic rocks dating back to 2.1 Ga, roughly coeval with those from BHT. Archean components are present in both Chinchaga domain and BHT, though their percentage contributions to the rock composition are marginally lower in the former domain [Ross *et al.*, 1991]. Chinchaga domain ends at STZ and sharply transitions to positive aeromagnetic and gravity values within a wedge-shaped Wabamun domain. The origin and age of Wabamun domain remain poorly constrained, though the impact of southwestern STZ, which bifurcates

around Wabamun domain, cannot be underestimated in the domain evolution. At the present time, the understanding of Wabamun domain heavily relies on the interpretations of the adjacent Thorsby and Rimbey domains, two southwest-striking magnetic and gravity lows that are generally associated with the complex convergence and transpression along the STZ [Ross *et al.*, 1995; Ross, 2000]. Reverse faulting [Ross *et al.*, 1995], magmatism and subduction may be required to explain the isotopic composition of the granitic rocks beneath Rimbey domain [Ross *et al.*, 2000].

Further east, the crustal signatures of central Alberta exemplifies the complex tectonic history of western North America. This region mainly resides in southern Hearne province, an Archean microcontinent as old as 2.8-3.5 Ga based on Zr and U-Pb analysis [Lewry and Sibbald, 1980; Frost and Burwash, 1986; Crocker *et al.*, 1993; Bickford *et al.*, 1994; Boerner *et al.*, 2000]. Despite a history that dates back to 3.0-3.5 Ga, much of the region underwent continental collision and intra-continental shortening during the early Proterozoic (1.7-1.9 Ga) [Ross *et al.*, 1995; Boerner *et al.*, 1995; Edwards and Brown, 1999; Ross and Eaton, 2002]. Recent tectonic models of Hearne Province suggest that central Alberta area underwent coeval subduction along STZ in the southwest and Trans-Hudson Orogen (THO) in the east [Ross *et al.*, 2000]. West of Hearne province, a subdomain directly affected by the Proterozoic collision is Eyehill high (EH), a 70-km long positive aeromagnetic anomaly approximately parallel to THO [Hope and Eaton, 2002]. The role of EH during the subduction of THO under Hearne Province remains debated.

The most significant subdivision of Hearne province is Loverna Block (LVB), a north-eastern striking Proterozoic block bordering with Lacombe, Rimbey and Thorsby domains. LVB may have undergone clockwise rotating centered at Bonnyville, a moderate-sized town in east-central Alberta [Boerner *et al.*, 1995]. Much of the rocks in this region are of Archean age [Villeneuve *et al.*, 1993; Ross *et al.*,

1991], though evidence from geophysical and geochemical analysis has suggested extensive rework during the Proterozoic eon [*Hoffman, 1988; Ross and Eaton, 1999; Boerner et al., 2000; Gorman et al., 2002; Clowes et al., 2002*]. The extent of reworking may have been sustained along the Lacombe domain, an elongated boundary zone between Hearne province and STZ. While Nd isotopic study indicates the presence of weakly metamorphosed volcanic and sedimentary rocks, the age of Lacombe domain is only roughly constrained to be Paleoproterozoic (less than 2.3 Ga) [*Villeneuve et al., 1993*]. The geographic position of Lacombe domain overlaps with the well-known Red Deer Conductor [*Boerner et al., 2000*].

Southern Alberta mainly consists of the VS, a narrow domain with prominent east-trending gravity and magnetic anomalies [*Villeneuve et al., 1993; Ross et al., 1991*], and a larger Medicine Hat Block (MHB) that extends into northwestern US. VS spans more than 350 km and cut cross the potential-field fabric of southern Alberta at a high angle [*Eaton et al., 1999b, 2000*]. Drill core samples from VS suggest an early Proterozoic (circa 1.8-2.7 Ga) origin [*Villeneuve et al., 1993*], but the interpreted age and genesis of VS differ considerably among earlier studies [*Lemieux et al., 2000; Eaton et al., 1999b*]. Equally controversial is MHB, a positive potential field anomaly flanked by VS and the Archean Wyoming province. MHB consists mainly of granitoid with ages ranging from 2.6 Ga to 3.2 Ga [*Villeneuve et al., 1993; Ross et al., 1991*], predating those beneath VS, and mid crust of MHB is inudated by west- and southwest- dipping reflection fabrics. The layered lower crust and geometric cutoffs of MHB are interpreted as the remnants of a complex geological framework [*Lemieux et al., 2000*]. Regional reflection profiling data favored an origin in connection with the assembly of two ancient Archean blocks [*Lemieux et al., 2000*], whereas potential Proterozoic collisions between LVB and the Archean Wyoming Province may also have played a role in its formation and evolution [*Eaton et al., 1999b; Mueller et al., 2002*]. Both scenarios would result

in crustal shortening, which would facilitate the formation of VS in the early Proterozoic. Additionally, post-collision injection of Mafic melts can also be traced to the crust beneath MHB and potentially extending to the basement structure of VS [Lemieux *et al.*, 2000; Mueller *et al.*, 2002].

3.2 Data and Methods

The data analyzed in this study consist of broadband recordings from 13 CRANE stations, 3 Canadian National Seismic Network (CNSN) stations and 7 US Array stations. With an average spacing of ~ 150 km, CRANE provides the primary crustal constraints in southern-central Alberta. The inclusion of the US Array, which operated in Montana during the limited time window from late 2007 to early 2009, is vital for the structural analysis beneath southern Alberta. To obtain correlation stacks between stations we 1) segment the piece-wise vertical component records into 12-hour intervals, 2) apply a low pass filter cornered at 1 Hz, and 3) bit normalize [Bensen and Ritzwoller, 2008] the filtered seismograms to minimize the effect of earthquakes and other high amplitude, non-ambient seismic signals. Cross correlation is subsequently performed on each station pair with overlapping time segments, and the results are stacked to improve the signal-to-noise (SNR) ratio. The average length of data that contributed to the correlation stack for each given station pair is ~ 1.5 years. While more than 300 hundred cross-correlation functions are computed using the above approach, 100 to 200 correlation stacks are eventually retained for each frequency range analyzed in this study after subjecting the results to an SNR test. Figure 3.2 shows CCFs with acceptable SNR ratios for tomographic inversions. The lag times of the correlation peaks are sensitive to the differential path structures from the seismic source to the two stations being correlated. Under the ambient noise source assumption, CCFs (and their derivatives)

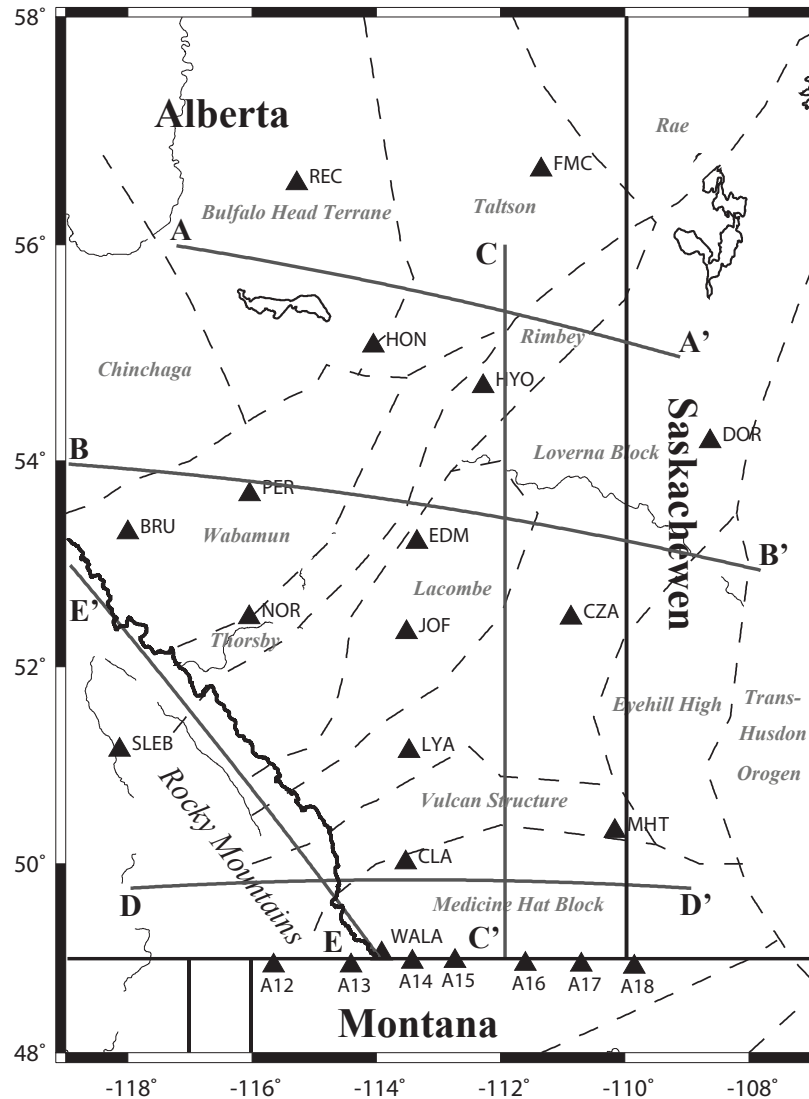


Figure 3.1: Distribution of stations (black triangles) from the Canadian Rockies and Alberta Network (CRANE) and nearby Canadian National Seismographic Network (CNSN). The dashed grey lines denote the known boundaries between tectonic blocks based on earlier geophysical and geological surveys [Ross *et al.*, 1991; Villeneuve *et al.*, 1993]. The solid gray lines denote the vertical cross sections in Figure 3.9 (see Section 3.4).

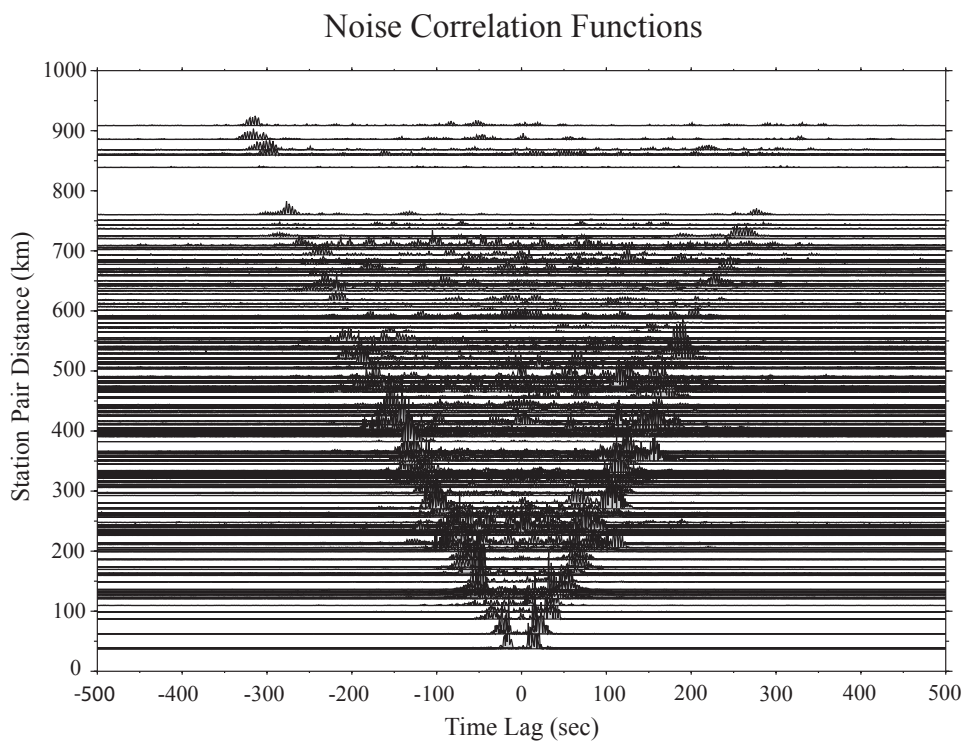


Figure 3.2: SCCFs computed for all station pairs. The peaks of the SCCFs increase linearly at an approximate speed of 3 km/sec.

become the effective Green' s functions between two stations and the lag times reflect the associated Rayleigh wave speeds [Yao *et al.*, 2006; Sabra *et al.*, 2005a]. The peaks in the CCF show semi-linear distance-time move-outs that are, to the first order, consistent with the ambient noise assumption. A sample CCF from two CRANE stations (Figure 3.3a) shows prominent noise correlation peaks that exhibit consistent positive and negative lag times relative to the origin. These peaks generally remain robust in a broad range of frequencies (Figure 3.3b) and enable accurate determinations effective Rayleigh wave group velocities [Lin *et al.*, 2008; Bensen *et al.*, 2007a; Shapiro *et al.*, 2005; Ritzwoller *et al.*, 2011]. The residual effect of secondary non-ambient sources [Gu and Shen, 2012], which is generally reflected in the slight asymmetry of the CCFs (see Figure 3.3b), are minimized by collapsing the positive and negative halves of CCFs for effective average measures of lag times. To maximize data coverage we compute broad band CCFs for all possible combinations of stations. These CCFs are then filtered to five narrow, slightly overlapping passbands of 0.002-0.04 Hz, 0.03-0.08 Hz, 0.06-0.12 Hz, 0.1-0.16 Hz and 0.14-0.2 Hz. Frequency bands used in this study translates to center periods of 50 sec, 20 sec, 10 sec 8 sec and 6 sec, respectively, for the five frequency ranges. These frequency ranges were selected based on simulated Rayleigh wave depth sensitivities using the Reflectivity Method [Choy *et al.*, 1980; Gu *et al.*, 2005; Gu, 2006; Fuchs and Müller, 2007; Ökeler *et al.*, 2009]. This computation assumes a stratified one-dimensional regional P velocity model [Bouzidi and Schmitt, 2002], scaled by a factor of 1.1 [Stein and Wysession, 2009] for shear velocities, and estimates the maximum numerical derivatives of the timing and waveform of Rayleigh wave at a given layer depth for a distance of 300 km. This procedure provides estimated depth sensitivities at the average distance between our receiver pairs. The eventual selection of the five narrow-band filters aims to provide a relatively uniform depth coverage down to 50-60 km depths while ensuring sufficient observations in

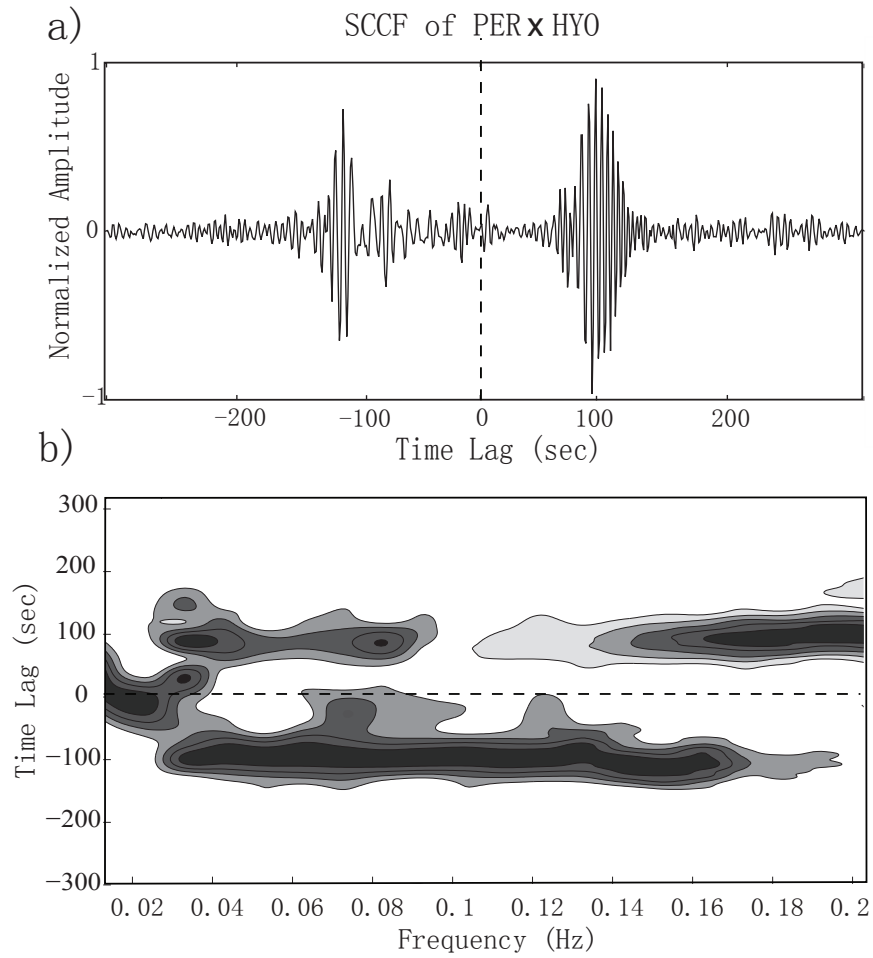


Figure 3.3: (a) Unfiltered SCCF between station PER and HYO. The average of forward and time-reversed SCCF peaks represents the effective Green's function between the station pair. (b) Effective dispersion curves of SCCFs within the frequency range of 0.015-0.25 Hz. The lag times of the correlation peaks reflect the effect of Rayleigh wave dispersion.

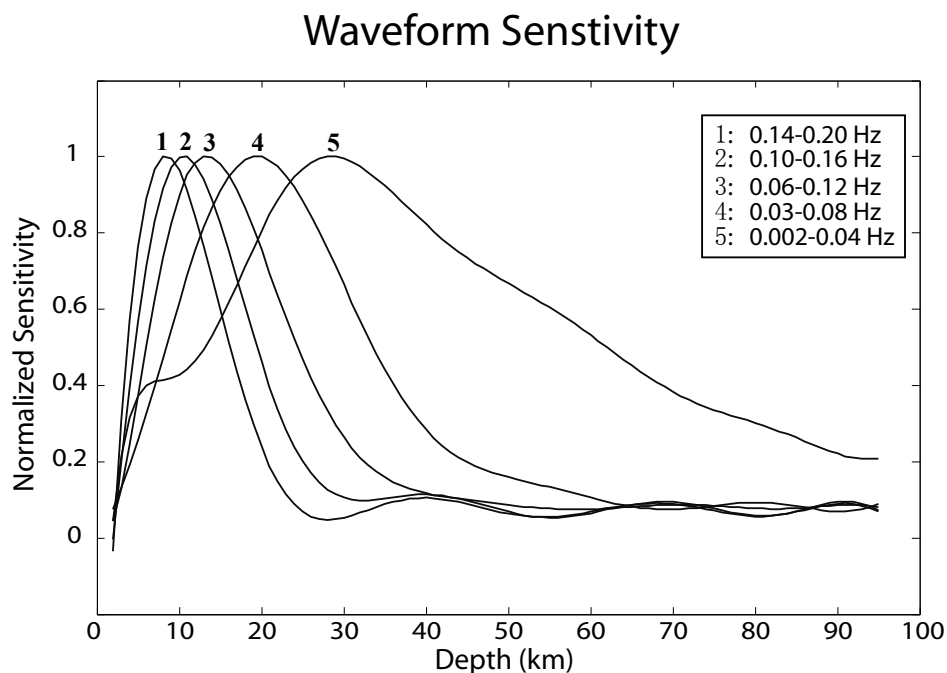


Figure 3.4: Normalized waveform sensitivities for the five frequencies used in this study. The values are computed based on the reflectivity methods and a scaled regional P velocity model [Kanasewich *et al.*, 1995].

each frequency range. The average Moho depth in the study region is 45-50 km [Bassin *et al.*, 2000; Gorman *et al.*, 2002; Gu *et al.*, 2011], which suggests that our CCF stacks are capable of constraining structures from the upper crust (highest frequency band) to the shallow mantle (lowest frequency range) beneath the study region (Figure 3.4); the best resolved region is the middle and lower crust (frequency ranges 2-4) due to greater data density and coverage. For each selected frequency range, correlation peaks of the envelope functions and group arrival times follow a linear move-out curve (Figure 3.5). The slope of the best-fit line over the time measurements provides an estimate of the average velocity for the frequency range. The intercept from linear regression is nonzero due to the presence of noise in the data as well as the associated uncertainties in time measurements and data distribution. The magnitude of the intercept, which should be as small as possible at zero

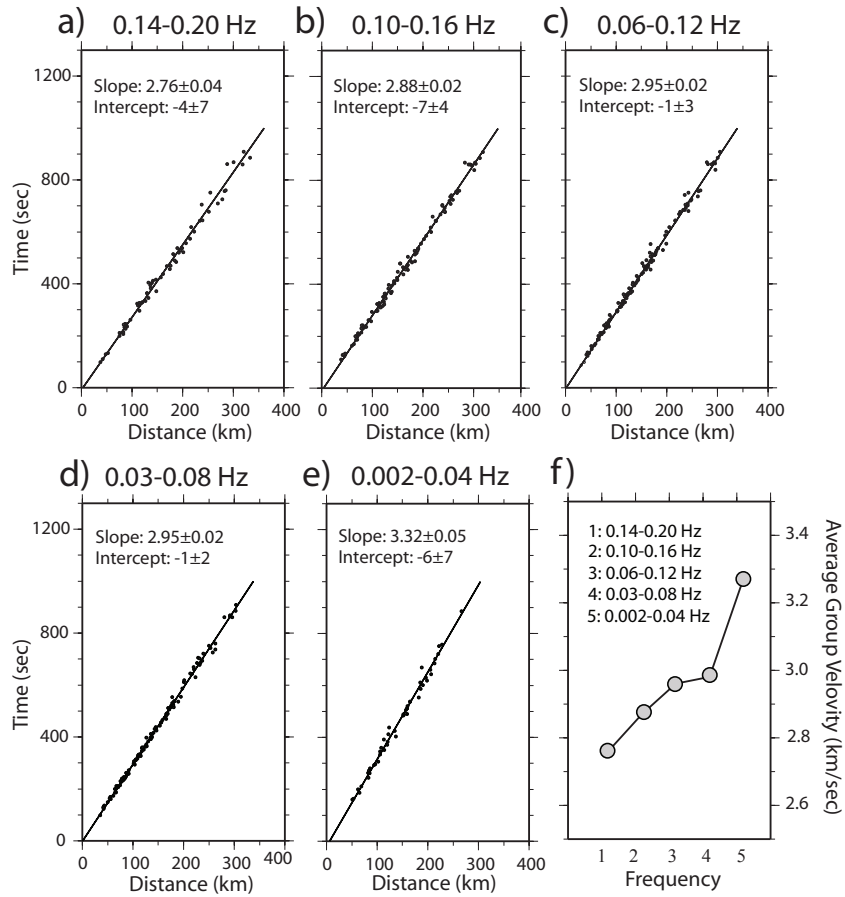


Figure 3.5: (a)-(e) Lag times of SCCF peaks for all five frequency ranges. The slopes of the linear plot are effective average velocities of the region at a given frequency, while the intercept of the least-squares fit shows the uncertainty of the average velocity and potentially biases in data quality and distribution. f) A comparison of the average velocities. The trend suggests increasing average crustal speeds with depth.

distance, is therefore a useful metric of the data quality. Thus more reliable measurements are obtained for the frequency ranges 1, 3 and 4 (Figure 3.5) without the consideration for the number of observations. The average velocities of all frequencies range from 2.8 km/sec to 3.2 km/sec (Figure 3.5f), which are consistent with earlier regional estimates [Kanasewich *et al.*, 1995; Clowes *et al.*, 2002] assuming a 0.92 scaling factor between Rayleigh and shear wave speeds [Stein and Wysession, 2009]. The low velocity shallow crust exhibits strong effects of sedimentary rocks in the Alberta basin.

We subsequently perform nonlinear, two-dimensional (2D) tomographic inversions using the lag time measurements from SCCF stacks. The inversion algorithm is based on the Fast Marching Method that utilizes the Fast Marching Surface Tomography Package [Rawlinson and Sambridge, 2005] to perform two-dimensional (2D) ray tracing and subspace inversions. Successful applications of this method can be found in crustal [Saygin and Kennett, 2012] and mantle [Saygin and Kennett, 2010] studies globally. To map the lag time measurements to velocities, we first discretize the study region into 1 deg \times 1 deg (latitude \times longitude) cell. The average group velocities (see Figure 3.5f) are used as the 1D reference model for the 2D inversion of lateral heterogeneities. The lag time measurements are subsequently inverted by updating both velocity and the 2D ray path [Rawlinson and Sambridge, 2005]. To minimize the effect of outliers, measurements with residual-to-distance ratios higher than 0.25 sec/km are eliminated during each iteration in well sampled regions; slightly higher cutoff values are adopted for regions with limited path coverage. This re-weighting procedure eliminates approximately 5-10% of all measurements.

Due to the presence of noise and limited data constraints, solution to the inverse problem is highly non-unique and requires additional regularization measures. The inversions in this study aim to minimize the sum of variances in data residual, model

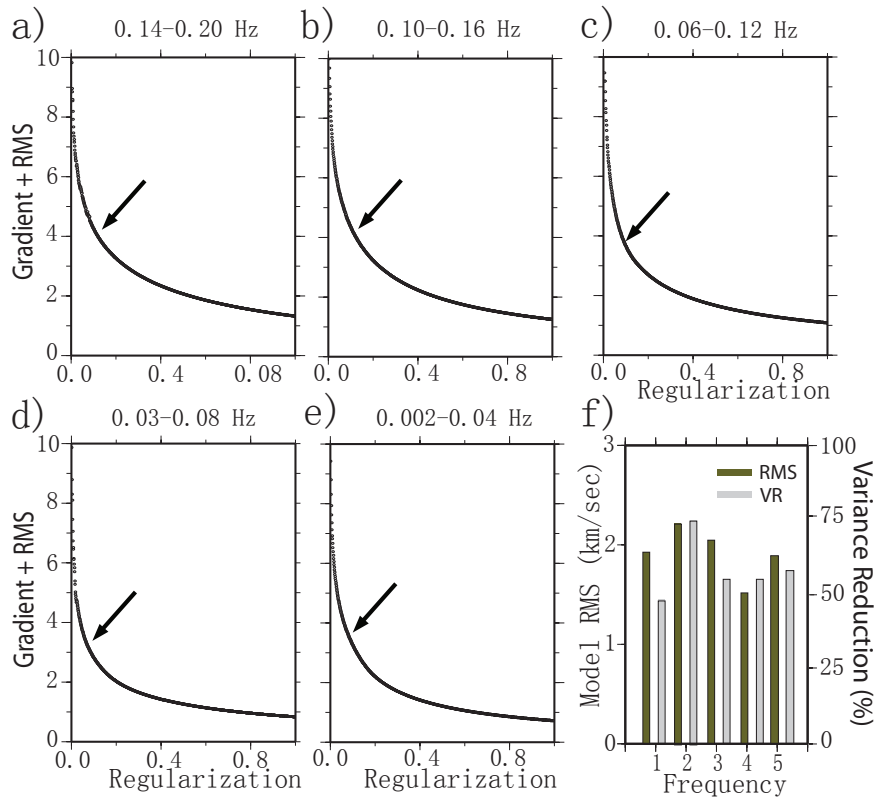


Figure 3.6: (a)-(e) Tradeoff curves of regularization factors (norm+Gradients) and model root-mean-squared (RMS) value. The regularization factors for the inversions are determined by the turning points. f) Reduction of data variance and RMS model velocities at all frequencies.

size and model gradient. For each frequency range, the latter two terms in the objective function are governed by norm and gradient damping parameters, respectively. Changes in the patterns of the model solutions are relatively minor for a broad range of damping parameters, whereas the amplitudes and gradients of seismic velocities vary as expected. We determine the optimal choices of damping from the turning points of their respective tradeoff curves with data fit [Tarantola, 2005]. For instance, values close to 0.05-0.1 are adopted as norm damping parameters in the inversions of all frequencies (Figure 3.6a-e). Reduction of data variance (for short, variance reduction) and root-mean-squared (RMS) model coefficients for each frequency band are shown in Figure 3.6f. The former quantity is computed based on

the residual lag times (data-model prediction) where data represent perturbations of path lag times relative to the reference structure. The variance reduction used in this research is defined as:

$$R = \left(1 - \sqrt{\frac{\sum_{i=1}^n (T_i^2 - T_i'^2)}{\sum_{i=1}^n T_i'^2}}\right) * 100\% \quad (3.1)$$

where T_i and T_i' are observed and model predicted lag times for the i^{th} station pair.

While fitting the absolute lag times between stations would yield variance reductions in excess of 90% for all station pairs, variance reductions (between 50% and 70%) of lag-time perturbations to the average velocities at each frequency (see Section 2) are more realistic estimations of the Green's functions between station pairs. Overall, the intermediate frequencies ranging from 0.1 Hz to 0.16 Hz are more confidently resolved than the two end frequencies. The RMS values of the lateral velocity variations range from 1.5 km/sec to 2.5 km/sec. The high frequency passbands (1-3) show greater RMS values than lower frequencies, which implies a strongly heterogeneous upper/middle crust.

3.3 Tomographic Results

3.3.1 Assessment of Data Resolution

To quantify the resolutions we perform standard checkerboard tests on all five frequency bands with initial cell dimensions of 1 deg (latitude) \times 1 deg (longitude). A correction factor was introduced to account for the slight decrease in actual cell sizes at larger latitudes [Rawlinson and Sambridge, 2005], and Gaussian noise equivalent of three seconds in lag time were added to the simulated lag times prior to the resolution test. The resulting checkerboards typically recover 60-65% of the input model amplitudes for frequency ranges 2-4, which are mainly sensitive to the upper to mid crustal depths (Figure 3.7a-c), and the positions of model extremes are consistent with those of the input checkerboard. Velocity structures south of

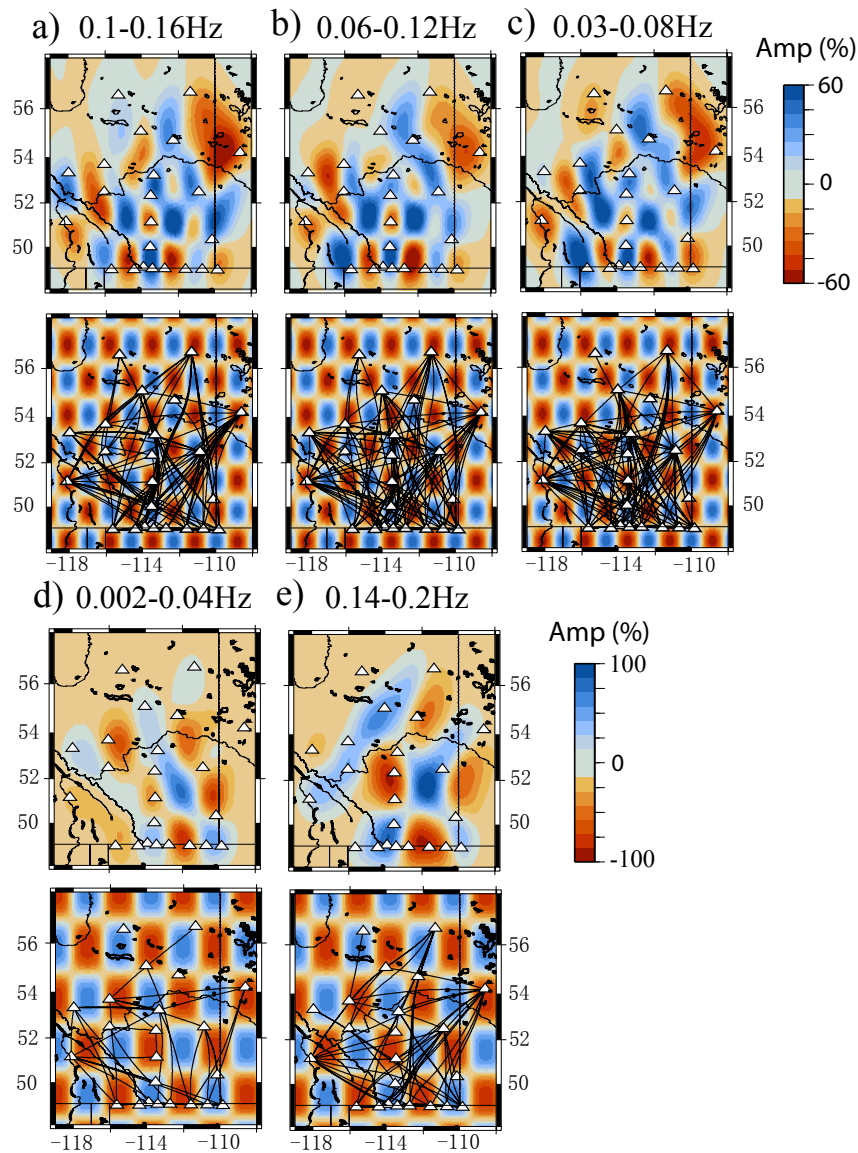


Figure 3.7: Resolution test for all five frequencies. The lower panels show the input checker-board pattern. The final SCCFs used for inversion are represented by the solid black lines connecting CRANE and CNSN stations (White triangles). A three sec white noise is added to the original model predicted values prior to inversions. Bigger gridsize ($1.5 \times 1.5 \text{ deg}^2$) is used for frequency ranges 0.002-0.04 Hz and 0.14-0.2 Hz due to limited numbers of quality SCCFs. Approximated 60% of the input amplitude is resolved for smaller grid size (a-c) while up to 90% of the input amplitude is resolved for the frequencies with coarser grid sizes (d and e).

Edmonton are especially well resolved, thanks to the added high-quality SCCFs in association with US array stations. On the other hand, the northern part of the array (above 52-deg latitude) shows notable smearing effects due to sparse path coverage. For example, station REC near the northwest corner of our study region only provides fewer than 10 quality SCCF measurements on average due to limited operation time between 2006 and 2007. The velocity beneath the Rockies are slightly better resolved than northern Alberta, despite relatively fewer stations, owing to the limited but robust measurements associated with SLEB. The two remaining frequency ranges, 1 and 5, are poorly resolved with grid sizes of 1 deg^2 due to limited path density (Figure 3.7d and e). The minimum resolvable cell size for these frequencies is $1.5 \text{ deg} \times 1.5 \text{ deg}$, as suggested by recovery of the input amplitudes by up to $\sim 80\%$ in southern central Alberta. Using the resolution tests as a guide, the remainder of this section will focus exclusively on the group velocities beneath areas that are adequately resolved in the five frequency ranges.

3.3.2 Group Velocity Maps and Cross-sections

The passband of 0.14-0.2 Hz is mainly sensitive to shallow crustal structures at 5-10 km depths (see Figure 3.4). The structure beneath Edmonton is, on average, $\sim 6\%$ slower than surrounding regions (Figure 3.8a). The elongated slow velocity zone roughly extends from the Rockies near BRU to northern-central Saskatchewan in the vicinity of DOR and is flanked by high velocity zones in the northeast of Edmonton and southern Saskatchewan river basin. The latter anomaly is, however, sharply cutoff by a well-resolved low velocity zone east of the foothills of the Rockies near Canada-US border, resulting in a velocity gradient in excess of 20% in MHB. The structure beneath the Rockies appears to be complex, exhibiting both low (under SLEB) and high (south of SLEB) velocities at shallow crustal depths. The average group velocity increases from 2.76 km/sec to 2.84 km/sec in the passband 0.1-0.16

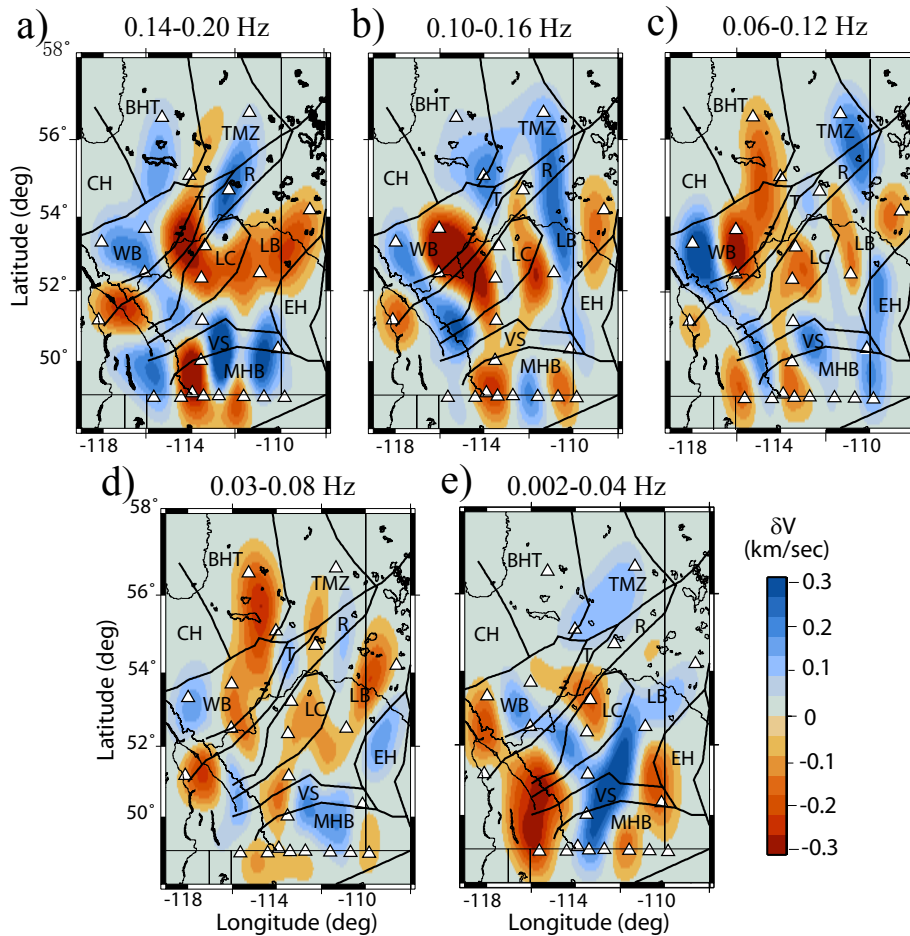


Figure 3.8: Tomographic results of the SCCF group velocity inversions. Velocities for each of the five frequencies are plotted as perturbation to the average velocities. The black lines denote the reported boundaries between known tectonic blocks [Ross *et al.*, 1991]. CRANE and CNSN stations used in this study are represented by white triangles.

Hz, which is mainly sensitive to the depth range of 8 to 12 km. While high velocities from shallower depths remain roughly unchanged at upper crustal depths beneath the northern Rockies (west of BRU), a low velocity zone east of the foothills in central Alberta (e.g. BRU and PER) become more prominent both in size and in amplitude relative to those in the shallow crust (Figure 3.8b). A north-south oriented, high velocity anomaly is observed near the border of Saskatchewan, segmenting the broad low velocity zone from western Saskatchewan to central Alberta from upper crust (see Figure 3.8a). Combining with a high velocity zone within the foreland belt of Rocky Mountains, this frequency range highlights a major structural difference between central Alberta basement rock (slow) and the surrounding regions (fast). In southernmost Alberta, the western part of MHB remains slower than average despite reduced east-west velocity gradient across it. This pattern continues down to mid and lower crustal depths in southern Alberta, where significant high velocity zones are observed along the foothills near the Alberta-British Columbia border and below-average velocities are present in southern-central Alberta (see Figure 3.8c). On the other hand, apparent velocities beneath TMZ and BHT become $\sim 5\%$ slower than the surrounding regions. This anomaly extends by 100-200 km southward, potentially connecting with reduced velocities in eastern Wabamun domain and central LVB (see Figure 3.8b). Similar structures are observed in frequency range 4, despite a visible loss of amplitude (Figure 3.8d), which suggests relative smooth transitions from mid to lower crustal depths. On the other hand, the seismic structures revealed by the longest periods (Figure 3.8e) are characteristically different from those shown in Figure 3.8a-d. This frequency range is primarily sensitive to depths from mid crust (~ 25 km) to Moho or upper mantle (~ 50 km) (see Figure 3.4) could be affected by the regional variations in Moho depth. The most prominent structure is a V-shaped high velocity zone that extends from MHB to Wabamun domain and central LVB, respectively, along northwest

and northeast orientations. The peak velocity at the center of the anomaly beneath LVB is $\sim 10\%$ higher than the regional average of 3.3 km/sec in the frequency range of 0.02-0.04 Hz. On the other hand, the foothills of the Rocky Mountains are underlain by low velocities, potentially reaching the base of the mountain belt near the US-Canada border. Below-average velocities are also observed in Lacombe Domain near station EDM, which is consistent with the overlying crustal variations from higher frequencies in the southeastern portion of the study region. Among the well-resolved regions, all five maps show consistent large-scale low velocity structure in southern central Alberta. The western part of MHB is generally underlain by below-average velocities, while central and eastern MHB are considerably faster in all five maps. Still, a number of heterogeneous structures are difficult to quantify or interpret: for instance, the wave speeds beneath the Rockies are highly variable among the different frequencies, which potentially reflect reduced lateral resolution due to the insufficient station coverage. In addition, the inverted velocities from passband 5 are strongly heterogeneous and the overall pattern is characteristically distinct from those of the remaining frequencies.

3.4 Discussion

The main objective of this study is to improve the knowledge of the crustal structure and history beneath central and southern Alberta, which is critical to the understanding of the formation and tectonic development of western Laurentia. The study region marks the transition from cratonic North America in the east/northeast to the accreted terranes in the west/southwest, with ages of basement rocks potentially ranging from the Archean to the Proterozoic. While parts of the crystalline basement in the region (e.g., LVB) are likely Archean below the thick Phanerozoic sedimentary cover [*Hoffman*, 1988, 1989], the crust may have been significantly

reworked due to a series of collisional, subduction, magmatic and metamorphic events since the Paleoproterozoic era [Burwash and Krupička, 1969; Ross *et al.*, 2000; Boerner *et al.*, 2000; Canil *et al.*, 2003]. Broadband ambient noise SCCFs documented in this study enable an up-to-date examination of the crustal and shallow lithospheric velocity variations beneath the study region. Peak-to-peak lateral velocity variations up to 0.6 km/sec at mid crustal depths are compelling evidence of the structural complexity beneath the platform sedimentary cover. The inverted regional crustal velocity structures are best constrained in southern Alberta and southeastern British Columbia. The average velocities increase at longer periods, as would be expected from the dispersion of Rayleigh waves, while a notable RMS amplitude reduction with depth and strong gradients in the patterns of lateral heterogeneities are potentially more informative of the regional crustal/upper mantle temperature, lithology and compositions [Holbrook *et al.*, 1992; Christensen, 1979; Barton, 1986; Brocher, 2005]. The following section provides an in-depth analysis of the key observations and their correlation with known geology and tectonic history of the study region. To facilitate the discussions we construct a 3D map of heterogeneities where value at a given depth represents the superposition of group velocity maps obtained from all five frequencies weighted by their respective sensitivities (see Figure 3.4). Due to the increasing half-widths of the sensitivity functions with depth, the 3D reconstruction slightly exaggerates on the sizes of major velocity anomalies below lower crust. The projection of the effective phase velocity maps mainly aims to provide a closer examination of the major velocity anomalies.

3.4.1 Northern Alberta

From the west to east, the northern cross-section of our study region (Figure 3.9AA') samples BHT, TMZ and northern Rimbey province in succession (see Figure 3.1). This section begins in southern BHT, a basement domain often grouped with the

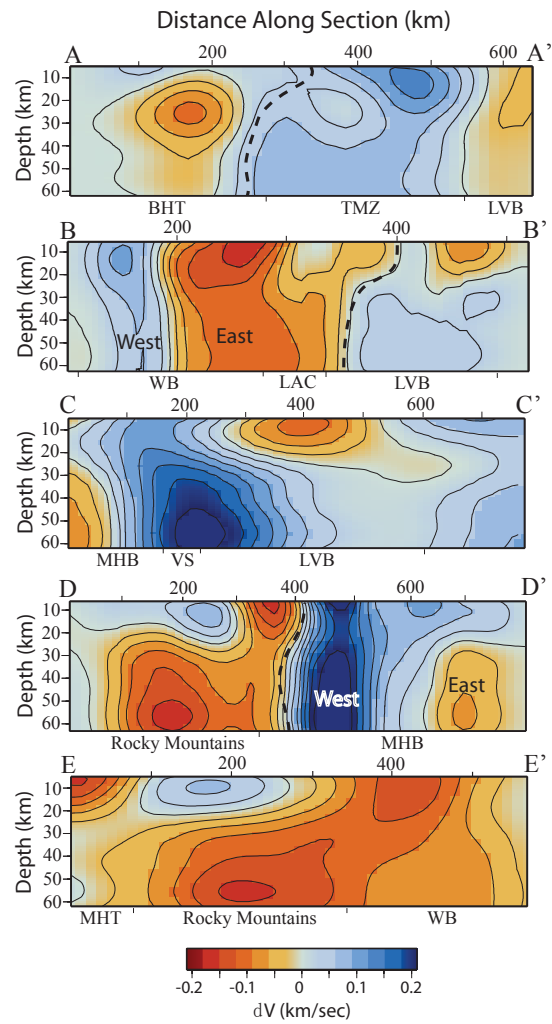


Figure 3.9: Estimated vertical cross-sections (see surface projection in Figure 1) of shear velocity perturbations relative to the regional averages. At a given depth, the contribution of a given frequency range is computed based on the corresponding sensitivity curve shown in 3.4.

adjacent Chinchaga domain as potentially rifted slivers near the southwestern margin of Rae province in circa. 2.3-2.0 Ga [Theriault and Ross, 1990; Villeneuve *et al.*, 1993]. Beneath the 1-2 km Phanerozoic cover, the crust consisting mainly of metaplutonic rocks ranging from gabbro to leucogranite [Theriault and Ross, 1990; Burwash and Krupička, 2000; Ersan *et al.*, 2009]. This region is well known for the diamondiferous Buffalo Head Hills kimberlite field, possibly formed during the late Cretaceous [Carlson *et al.*, 1999; Eccles and Heaman, 2003] petrogenesis of the northern Alberta kimberlite province. The westernmost segment of cross-section AA' shows a distinct low velocity zone in the vicinity of BHT at depths from mid to lower crust. The top of the anomaly (subjectively defined by 3% value) is 10-15 km, while velocities gradually increases downwards to reach a maximum value of 3.2 km/sec at ~25 km. The depth extent of this structural anomaly remain the unclear: while low velocities do not extend beyond 40 km in the present model, earlier inversions that included two large station residuals in connection with REC resulted in anomalously low velocities in the group velocity map of 0.02-0.03 Hz, or lithospheric mantle [Shragge *et al.*, 2002]. The top of the slow anomaly is interrupted at depth of 15-25 km, which overlaps with the reported range of the Winagami reflection sequence. Should an intrusive sill be responsible, the termination of the observed anomaly at shallow crustal depths would imply interrupted flow at the brittle-ductile transition in mid crust. This interpretation remains speculative, however, as the low-velocity anomaly is less imposing than the reported sill layer that covered an area $> 12,0000 \text{ km}^2$ [Ross and Eaton, 1997]. An alternative explanation of non-sill mafic crust [Villeneuve *et al.*, 1993] remains a possibility. In either scenario, it is plausible that the imaged low velocity anomaly is only a constituent of a larger, more significant anomaly under BHT that underwent subduction [Davies *et al.*, 2004; Banas *et al.*, 2007; Ersan *et al.*, 2009] during the Archean [Janse, 1994], reworking during the Proterozoic [Aulbach *et al.*, 2004; Ba-

nas et al., 2007] and, more recently, magmatism and mantle upwelling during the late Cretaceous [*Carlson et al.*, 1999; *Eccles and Heaman*, 2003; *Hood and McCandless*, 2004; *Davies et al.*, 2004]. In comparison, the eastern part of the low velocity zone is well constrained by the noise-correlation observations and appears to terminate upon entering TMZ. The crustal velocity under TMZ (see Figure 3.9AA') is slightly higher than the regional average (~ 2.9 km/sec), resulting an eastward velocity increase of 0.4 km/sec from southern BHT to western TMZ. This structural gradient is partially supported by the regional aeromagnetic signatures [*Ross et al.*, 2000; *Pilkington et al.*, 2000], a key metric adopted in the original definition of the domain boundaries. The absence of distinctive low-velocity crustal signatures in TMZ, as would be expected from strong thermal energy sources [*Bachu*, 1993], is enigmatic in view of TMZ's similar crustal age and potential association with BHT [*McNicoll et al.*, 2000]. Assuming TMZ was a composite continental magmatic arc and collisional orogen during the Proterozoic BHT- Hearne collision [*Ross et al.*, 2000], the near-average crustal velocities (see Figure 3.8) would suggest the absence of present-day thermal or compositional bulk crust in its southern half. Two additional stipulations could be made based on the inverted velocities: 1) strong geothermal energy reported [*Bachu*, 1993; *Majorowicz and Moore*, 2008] in southern TMZ is most likely limited to depths or spatial scales beyond our seismic resolution limits, and 2) the mid crustal low velocity zone in BHT resulted from recent (e.g., Cretaceous) magmatic events that had little or no bearing on the structure beneath TMZ.

Cross-section AA' continues through the northern part of Thorsby and Rimbey domains in Alberta and shows a significant increase in shallow crustal velocities. Centered between 10 and 15 km depths, the teardrop-shaped high velocity zone dips northeastward (see Figure 3.8 and Figure 3.9AA') along the Rimbey-Loverna domain boundaries, which highlights the structural gradient between mildly above-

average crustal velocities in southern TMZ and slow velocities in central LVB. The shape and position of this high velocity zone are sufficiently resolved by the noise records (see Figure 3.7), though slightly greater depth uncertainties (~ 10 km) would be expected. Rimbey domain was initially recognized by semi-linear, moderately intensive aeromagnetic anomalies along the western margin of Hearne province. Core samples of undeformed biotite monzogranite with ages between 1.78 and 1.85 Ga [Villeneuve *et al.*, 1993; Burwash and Muehlenbachs, 1997; Ross *et al.*, 1991; Ross, 2000; Boerner *et al.*, 2000], seismic reflection line [Eaton *et al.*, 1999a; Zelt and Ellis, 1989], and potential field and isopach/facies maps from the region are generally suggestive of a plate-boundary, subduction-related origin ([Ross *et al.*, 1995; Berman and Bostock, 1997]). However, the state of present-day crustal velocities and latitudinal variations within the domain remain inconclusive. Unlike the low-velocity dominated southern part (see section 3.4.3), there are no discernable connections between the high velocity zone beneath northern Rimbey and average-to-lower crustal velocities expected from magmatism induced by Proterozoic subduction which would presumably translate to lower or average crustal speeds [Cassidy, 1995; Eaton and Cassidy, 1996]. The extent of Proterozoic subduction in this region remain debated, as a recent electromagnetic synthesis [Boerner *et al.*, 2000] provides compelling evidence for a clockwise rotation of Hearne [Welford and Clowes, 2006] in response to coeval subduction along THO and STZ. The reported rotation pole (near Bonnyville, Alberta) implies significantly less domain-boundary consumption near northern Rimbey than its southern counterpart. In view of the extensive history Hearne province that began as early as 3.5 Ga ago (e.g., [Lewry and Sibbald, 1980; Crocker *et al.*, 1993; Bickford *et al.*, 1994]), it is plausible that a surviving piece of relatively intact (hence seismically fast) Archean crust from Hearne province is responsible for the observed high-velocity structure. This assumption does not necessarily conflict with the hypothesized Pro-

terozoic magmatism, as the shallow (upper-crustal) depth of the observed anomaly would imply a later emplacement during the tectonic reworking [Ross *et al.*, 2000] in the WCSB. Further discussions will be provided in the section below pertaining to southern Rimbey and STZ.

Cross-section BB' presents an in-depth look at central Wabamun domain (Figure 3.9BB'), the western segment of the most pronounced low velocity zone in the regional group velocity maps (see Figure 3.8). Central Wabamun is divided equally into two distinct halves, as the velocity contrasts at shallow crustal depths between a fast western segment near the foreland belt of the Rocky Mountains and an anomalously slow eastern segment with velocities below 2.5 km/sec. The strong gradient in velocity potentially places a potential seismic constraint on the crustal structural boundary between Wabamun domain, an aeromagnetic high [Ross *et al.*, 1991] with a west-trending low-velocity zone [Zelt and Ellis, 1989; Eaton *et al.*, 1999a; Ross *et al.*, 2000] and the adjacent Chinchaga domain/Rocky Mountain foreland belt with aeromagnetic low susceptibilities [Ross *et al.*, 1991; Villeneuve *et al.*, 1993]. A strong east-west crustal variation is partially supported by a strong potential field in eastern Wabamun. If this velocity gradient marks the true domain boundary, then Wabamun-to-Chinchaga/Rockies transition would be less continuous than those suggested by earlier reports based on active source seismic lines [Ross and Eaton, 2002], and the structurally coherent part of the Wabamun domain is at least 20-30% smaller than the existing domain boundaries (e.g., [Ross *et al.*, 1991]). These low velocities appear to extend beyond 60 km depth and potentially represent a crustal expression of a deeper, stronger low velocity zone at 100-300 km depths [Shragge *et al.*, 2002].

3.4.2 East Alberta Orogen and Snowbird Tectonic Zone

The low velocity zone under eastern Wabamun continues through Thorsby and Rimbey Province, eventually terminating in eastern Lacombe domain. The local minimum resides at a shallow crustal depth in the Wabamun-Thorsby boundary zone and at shallow crustal depths, showing consistent location and westward dip with those of a reported steep northeast-southwest velocity gradient [Ross and Eaton, 2002]. The broad low velocity zone suggests diminished structural variations across STZ, an elongated geological structure locally defined by Thorsby domain and bifurcates around a lozenge-like Wabamun domain [Ross *et al.*, 1991; Villeneuve *et al.*, 1993; Hanmer *et al.*, 1995; Flowers *et al.*, 2006; Berman *et al.*, 2007], and the adjacent Rimbey and Lacombe domains. This finding is consistent with a common collisional origin, as all aforementioned domains have been linked to East Alberta Orogen [Ross *et al.*, 1995; Berman *et al.*, 2007] and the coeval subduction during the development of the tectonic vise [Eaton *et al.*, 1999b; Ross *et al.*, 2000] in the Proterozoic. The contrasting seismic velocities beneath northern (fast) and southern (slow) Rimbey and nearby domains shed new lights on the nature of STZ across Alberta. As a highly controversial geological structure across much of the landmasses of Canada, the origin of STZ has widely been associated with collisions between Rae and Hearne provinces nearly 1.9 Ga ago [Berman and Bostock, 1997]. Various candidate mechanisms have been proposed, mostly notably shear deformation at ~ 2.6 Ga [Hanmer *et al.*, 1995], subduction during the Proterozoic [Ross *et al.*, 1991; Eaton and Cassidy, 1996], or incipient rifting on an old, 2.5 Ga orogenic belt [Flowers *et al.*, 2006]. Multiple mechanisms may be needed to explain the noise-correlation observations that are sensitive to the past microcontinent geometries and motions. The extensive low velocities in southwestern STZ favour a mechanism involving extensive crustal metasomatism and possible serpentiniza-

tion [Eaton and Cassidy, 1996] of oceanic lithosphere during the Proterozoic. On the other hand, due to its short distance to the rotational pole of Hearne, northeastern STZ in Alberta may have undergone limited subduction/modification during the same eon as well as limited overprinting at later stages, thereby preserving much of the deformation sustained during earlier episodes of rifting and shearing.

3.4.3 Central Alberta

A region of significant tectonic implications for the Proterozoic formation of Laurentia is Lacombe domain, situated at the southwestern edge of Hearne province [Hoffman, 1988; Ross *et al.*, 1991]. Core samples from this region mainly consist of low-grade supracrustal, metasedimentary and felsic metavolcanic rocks [Ross *et al.*, 1991], which have been associated with Paleoproterozoic origin [Villeneuve *et al.*, 1993]. The crustal velocities beneath Lacombe Domain (see Figure 3.8) are generally below the regional average, showing minimal variations from the neighboring domains in the west. Serpentinization from a southeast dipping subducted oceanic plate has been invoked to explain the strong mid-crustal low velocity zone [Holbrook *et al.*, 1992; Van Avendonk *et al.*, 2011] from receiver functions below EDM station [Cassidy, 1995; Eaton and Cassidy, 1996]. In comparison with the reported velocities from receiver functions, our group velocity maps favor lesser, but more evenly distributed, serpentinite in the crust. Further work is needed to quantify the effects of damping and adopted nominal resolution. It has been widely accepted that Wabamun Domain, Hearne province and THO underwent coeval subduction processes during the late Archean and early Proterozoic [Ross *et al.*, 2000; Eaton *et al.*, 1999b]. The similarity in the lower crust and lithospheric shear wave velocities between Wabamun and Lacombe domains is further evidence of a common origin. Ross *et al.* [2000] interpreted the Rimbey granite, which can be partially traced between Lacombe and Wabamun Domains, as subduction-related igneous

rocks resulting from a southeast subducting oceanic crust beneath Hearne province. Therefore, it is plausible that the low velocities covering Lacombe domain and part of Wabamun domain result from relic oceanic crust transported from latter domain to Hearne province during the Proterozoic collision. In such a scenario, the effective area of the oceanic basin rifted by the subduction may be comparable to the size of the low velocity anomaly.

The eastern boundary between Lacombe domain and LVB, the largest of the three constituents of Hearne province, is recognizable from the group velocities in the lower crust and upper mantle (see Figure 3.9BB'). The upper crust beneath LVB is dominated by two low velocity structures (see Figure 3.8), with the minimum value reaching as low as 2.4 km/sec at 8-km depth beneath western Saskatchewan (Figure 3.9CC'). Variations of the granitic rocks beneath LVB have been suggested earlier [Ross *et al.*, 1991], with ages ranging from Neoproterozoic to Paleoproterozoic, and the observed low seismic velocities are consistent with results from the LITHOPROBE SARAX experiment [Clowes *et al.*, 2002]. Thick Phanerozoic sediments in the basin could be a contributing factor at shallow crustal depths, mainly affecting high frequency (hence shallow depth) surface waves in this study. On the other hand, the lower crustal and upper mantle structure beneath LVB generally show faster velocity than the regional average (see Figure 3.8). The prominent feature results from 0.002-0.04 Hz inverted noise correlation map is a pronounced high velocity structure beneath LVB and VS, which is well resolved by the dense network of paths based on the successful recovery of a hypothetical structure similar to the observed (Figure 3.10). Positive velocities at frequency 0.002 Hz to 0.04 Hz approximately orient along the strike of LVB dominate the pattern of the long period surface wave map. Due to the surface wave dispersion (see Figure 3.4), this anomaly is a reflection of integrated seismic velocities in the depth range of 30-60 km as well as the depth of the Moho.

Formed in the late Archean, Hearne province went through dramatic rework during the mid Proterozoic eon. It was proposed that Wabamun domain and Western Trans-Hudson provinces both collided with Hearne province, resulting a collisional Plateau surrounded by dual subduction zones during the Proterozoic (e.g., [Ross *et al.*, 2000]). Though debated [Aspler *et al.*, 2002], the thickened lithosphere could become gravitationally unstable, causing a high velocity lithosphere to delaminate from the base of LVB [Shragge *et al.*, 2002]. The observed high velocity anomaly could represent the undeformed part of Archean Hearne crust, while its orientation is consistent with the proposed clockwise rotation of Hearne province [Boerner *et al.*, 2000]. More discussion about this anomaly will be presented in the later part of the discussion.

Finally, above-average upper crustal velocities are observed beneath EH, a positive aeromagnetic anomaly in the southeastern margin of Hearne province. Evidence based on Zr dating suggested a Paleoproterozoic age as the result of crustal shortening [Ross *et al.*, 1995]. Recent tectonic model shows EH is overlaying LVB along an eastward dipping reflector [Hope and Eaton, 2002], which is consistent with our observation of a velocity jump at shallow crust depths in potential connection with high-grade (granulite and amphibolite) facies metamorphic rocks [Ross *et al.*, 1991; Holbrook *et al.*, 1992; Ross and Eaton, 1999]. Our study provides further insights on the role of EH in the subduction along the THO [Ross *et al.*, 2000; Boerner, 1999; Boerner *et al.*, 2000; Németh *et al.*, 2005]. For instance, despite both being considered parts of the overriding Hearne province in the coeval subduction of Wabamun domain (west) and Superior province (east), the marked difference in crustal velocities between EH (high) with Lacombe (low) clearly suggests distinct processes that governed their formation and the subsequent tectonic reworking [Burwash *et al.*, 1973; Ross and Eaton, 1999; Ugalde and Underhay, 2008; Burwash and Krupička, 1969, 1970; Ross and Eaton, 1999]. It remains

unclear whether EH represents a part of reworked Archean crust along the THO [Clowes *et al.*, 2002] or, possibly, a remnant of the Superior province east of THO as a rifted margin since the late Proterozoic. The lower crustal and upper mantle velocities beneath EH are lower than the regional average. At these depths, a major contribution would be expected from THO, which may be traced down to 70-80 km depths beneath the western part of EH and southeastern Hearne province. Since THO is younger than Hearne province, the associated velocities are expected to differ between these two domains [Bickford *et al.*, 1994; Németh *et al.*, 2005]. In other words, the observed contrast in the velocities between upper/mid and lowermost crust could represent the structural transition between two welded tectonic regimes.

3.4.4 Southern Alberta

VS is a major tectonic boundary between LVB and MHB which features prominent east-trending gravity and magnetic variations. Its origin remain debated among competing hypotheses between a failed Proterozoic rift [Kanasewich *et al.*, 1969] and a large magmatic Proterozoic suture [Thomas *et al.*, 1987] between MHB and LVB. The VS is nearly indistinguishable from LVB at depths below 25 km, whereas a major northward velocity decrease in the upper crust (see Figure 3.9CC') potentially marks the seismological domain boundary. South of VS, a pronounced high velocity lower crust layer (HLCL) continues across western MHB along its northeast-southwest strike (see Figure 3.9CC'). The orientation, strength and continuity of this structure, which are well resolved based on the data coverage (Figure 3.10), make a compelling argument for a southward extension of the undeformed part of Archean Hearne province. The origin of VS, a proposed deformation complex, remains debatable since domain's effective depth is mainly confined to the top 20-30 km [Clowes *et al.*, 2002] of the crust. The contrast between the upper

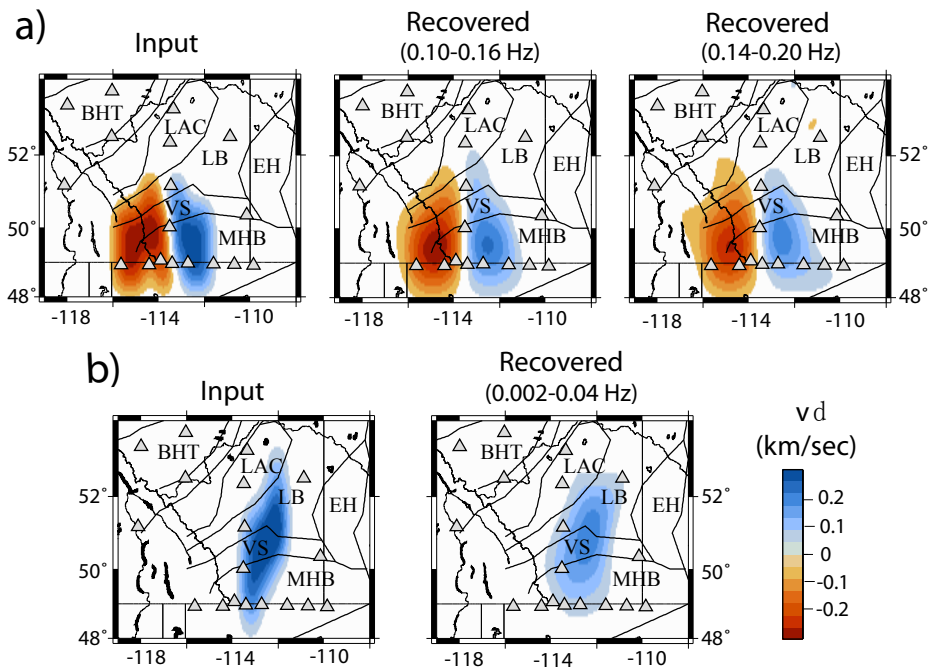


Figure 3.10: Resolution tests based on hypothetical structures similar to the observed. (a) Results of a test that assumes an input high velocity anomaly between western MHB and Eastern MHB. The pattern is well resolved at frequency ranges of 0.10-0.16 Hz and 0.14-0.20 Hz. (b) Results of a test with an input high velocity structure across LVB and Vulcan structure. Both the amplitude and the oblique orientation of the input model is sufficiently recovered by the SCCFs at 0.002-0.04 Hz.

(low velocity) and lower (high velocity) crust beneath VS is a potential indicator of differences in crustal history and/or composition.

The boundary between VS and MHB is not clearly defined by the crustal velocities despite earlier evidence of relatively older rock samples (~ 3.2 Ga; [Gorman *et al.*, 2002; Villeneuve *et al.*, 1993]) from the latter domain. It was proposed by Lemieux *et al.* [2000] that MHB was the amalgamation of two domains in mid Archean (circa 2.6 Ga). In its southern boundary, MHB is interrupted by GFTZ, a suture zone between MHB and Wyoming province with a significantly younger reported age than both domains [Mueller *et al.*, 2002]. This finding provided the basis for the hypothesis that MHB was originally a part of the Archean Wyoming province [Henstock *et al.*, 1998; Boerner *et al.*, 1998; Clowes *et al.*, 2002]. In this study, the southern most part of AA' cross-section reaches the US-Canada border and is constrained by relatively dense path coverages near the center of MHB. The resulting model shows large positive values, which are further illustrated by a east-west cross-section (see Figure 3.9CC') within MHB. The lower crustal/upper mantle velocities beneath MHB are comparable to those beneath southern Loverna Block and VS, two adjacent domains dominated by the distinctive HLCL (see Figure 3.9DD'). The strength and continuity of the HLCL in northwestern MHB makes a compelling argument that MHB was originally an integral part of, or had been strongly influenced by, Hearne province.

Validation of the potential connection between Hearne province and MHB would require a higher imaging resolution than achievable by this study to south of the US-Canada Border (Figure 3.10b). Further inquiries pertaining to the formation and integrity of the MHB remain debatable. For instance, based on the earlier SAREX experiment, western MHB poses the fastest relative P wave travel times in the crust [Clowes *et al.*, 2002]. However, the above-average velocities in MHB in this study mainly concentrates near the center of the southern Loverna block-VS-

MHB junction, while the eastern end of CC' (see Figure 3.9CC') is inhabited by weakly positive speeds in the lower crust. The limited thickness (~ 8 km) of the proposed HLCL by *Lemieux et al.* [2000] may negatively impact the layer detectability due to strong depth averaging in surface waves (see Figure 3.4). Still, the contrasting average lower crustal/upper mantle velocities between eastern (slow) and western central (fast) MHB require a satisfactory explanation. Barring significant tectonic reworking during the Phanerozoic era, such differences would favor MHB as the amalgamation of an Archean western-central fragment and a significantly younger/slower eastern segment. In view of the nearby EH, the latter segment was likely formed during the Proterozoic eon in connection with THO.

3.4.5 Rocky Mountains

Finally, our noise correlation tomography provides new and improved regional constraints on the craton -domain transitions. Of the five major Oregon-parallel morphologic belts [*Monger et al.*, 1982] of the Canadian Cordillera, our station coverage is mainly sensitive the Foreland belt. As the effective western boundary of the WCSB, the basement rocks in this region are generally believed to have formed in the late Cretaceous and early Tertiary during the Laramide orogeny [*Livaccari et al.*, 1981; *Maxson and Tikoff*, 1996; *English and Johnston*, 2004; *Cook and White*, 2010; *Liu et al.*, 2010]. Regionally deep Moho interfaces have been observed [*Shragge et al.*, 2002; *Mercier et al.*, 2008; *Gu et al.*, 2011] and interpreted as the isostatic response to loading of the lithosphere by Mesozoic thrust sheets (e.g., [*Monger et al.*, 1982; *Cook and Van der Velden*, 1993]), though the cause of the Laramide phase of mountain building and its effect on crust/lithosphere thickness remains uncertain [*English and Johnston*, 2004; *Liu et al.*, 2010]. Seismic velocities documented by passive source imaging [*Grand et al.*, 1997; *Simons et al.*, 1999; *Clevede and Megnin*, 2000; *Frederiksen et al.*, 2001; *Fouch and James*, 2004;

van der Lee and Frederiksen, 2005; Nettles and Dziewonski, 2008] have consistently suggested a major structural gradient from Phanerozoic mantle to cratonic lithosphere. However, the precise spatial location of this gradient, which is generally associated with the Cordilleran Deformation Front (CDF), is still in question due to the limited regional data coverage (e.g., [*Hyndman and Lewis, 1999; Lewis et al., 2003; Flück et al., 2003; Jones and Ledo, 2005; van der Lee and Frederiksen, 2005; Audet et al., 2007; Mercier et al., 2008*]). Our model presents improved regional constraints on the southern CDF. With few exceptions (e.g., near VS), the crustal velocity beneath the foothills of the Canadian Rockies are consistently lower than those beneath the adjacent Alberta basin (Figure 3.9EE'). A structural transition of $\sim 18\%$ in shear velocities occurs within lateral distances of 100-200 km, most notably at depths below mid crust. This result is in generally agreement with earlier regional surveys by *Clowes et al. [1995]* and *Zelt and White [1995]*, and the spatial location overlaps with a low velocity zone in the shallow mantle P velocities by *Mercier et al. [2008]*. However, due to the limited model sensitivities at depths below 60 km, the vertical extent of this low velocity zone [*Zelt and White, 1995; Mercier et al., 2008*] invites further investigations.

3.5 Conclusions

This study presents a new crustal velocity model of the southern WSCB based on the cross-correlation of the seismic noise between broad-band seismic stations. The density and coverage of SCCFs enable tomographic imaging at effective lateral resolutions of 1.00-2.25 deg² and depth sensitivities from 5 to 60 km. The best constrained part of the model is south of Lesser Slave Lake, where the majority of domain structures are well resolved at various crustal and shallow mantle depths. Summarized below are the key observations and associated interpretations.

1. Lower-than-average upper and mid crustal velocities beneath the LVB, which covers much of central and southern Alberta, reflect the depth-integrated effect of thick Phanerozoic sedimentary layer in Alberta basin. The structure changes sharply in the lower crust and shallow mantle, however, where a pronounced high velocity zone is identified in southern LVB. The orientation and amplitude of the anomaly suggests the presence of undeformed core of Hearne province, potentially formed in the Archean, underwent a clockwise rotation. The depth extent of the high velocity structure remains unclear.

2. Anomalously high lower-crustal velocities from LVB extend into MHB, which suggests a possible association of MHB with the formation of the Hearne province. Furthermore, the low velocity crust around this anomaly could be strongly influenced by the coeval subduction between Wabamun, LVB and THO during the Proterozoic eon.

3. The seismic velocities are highly variable within the MHB. The westernmost MHB is significantly slower than central MHB in the lower crust, which may imply the amalgamation of two distinct Archean blocks. The lack of distinctive velocity change between VS and MHB in the lower crust part also suggests the VS as a deformation complex confined to the upper and middle crust.

4. The Wabamun Domain shows consistently low crustal velocities, but the effective area is smaller than previous estimations.

5. The crustal velocities along the Canadian Rockies is considerably lower than the surrounding regions, which highlights a strong velocity gradient from cratons to terranes along the Cordillera Deformation Front.

6. The origin of the STZ remains in question, especially in view of strong north-south variations within Alberta.

Overall, the results of noise tomography reveal complex crustal structures and domains in Alberta. While the origins of many observed features remain largely

speculative, the improved data coverage based on regional arrays does, and will continue to, provide critical insights to the formation and evolution of western Laurentia.

Chapter 4

Conclusion

This thesis presents the first in-depth ambient noise correlation analysis across southern West Canadian Sedimentary Basin. Though partially revealed by the previous geophysical, surface geological and geochemistry researches, the crustal structures and tectonic histories of southern WCSB were still poorly constrained to date. Until recently, the deployment of the semi-permanent CRANE seismic network enables the possibility of an integrated, comprehensive study on the seismic structure of the basement of Alberta down to upper mantle depth. The main purpose of this thesis is showing the results revealed by analyzing SCCFs of correlating Crane, CNSN and US-array station pairs. Results of this thesis includes documentation of the seismic signatures of a persistent microseismic noise source originated from Lesser Slave Lake and a regional scale seismic velocity model for southern WCSB. A summarization of the findings from each approach in the previous part of this thesis will be listed in the later part of the text. Some of the results have been published in peer-reviewed journals (Chapter 2) and the rest have been submitted (Chapter 3). The process of noise-correlation consists of 3 parts before being subject to further analysis: 1. Signal station data preparation. Continuous recordings extracted from each individual stations are subject to band-pass filtering and bit-normalization for the purpose of eliminate influences of large earth quakes which would have a potential of biasing the results of noise-correlation. 2. Cross-

correlation of noise recordings. Each station pair shares an overlapped functioning time windows is processed by cross-correlation algorithm *Bensen et al.* [2007b] 3. Lag time and dispersion curve measurements. SCCFs computed in step 2 are filtered through a quality control process facilitated by interpolated dispersion curve (Figure 2.3 and 3.3). Quality SCCFs are later utilized for noise source analysis and Rayleigh wave travel time inversion.

Chapter 2 documents the seismic signatures of a persistent microseismic noise source revealed through the directionality analysis of SCCFs associated with station HON. It's revealed Lesser Slave Lake, the biggest water body in northern/central Alberta is producing constant microseismic noise detectable across the province. Seasonal and diurnal test suggests the noise source is more prominent through the winter season which can be the results of the unique winter environment of northern Alberta. Chapter 3 presents the results of travel time inversion applied on the symmetric SCCF measurements. Our tomographic model is tested to afford lateral resolutions of 0.5-1.0 deg² and depth sensitivities from 5 km to 60 km. The majority of the domains in the south of latitude 52 degree are well constraint due to the dense coverage of broadband seismic stations. Key findings of this study include a speculative core of the undeformed Archean hearne province detected beneath the modern day LVB. MHB, which was previously suggested to be the results of amalgamation of two ancient Archean blocks, highlights a major contrast in the velocities between western and eastern parts of the domain. Also, Wabamun Domain is resolved to be in much smaller scale than previous reports and the crustal velocities along the Rocky Mountains are found to be slower than surrounding areas. The surface velocity documented in this thesis presents similar range and average value compare to other region with analogous history and crustal structure as Mexico bay [*Godey et al.*, 2003; *Zhang et al.*, 2007], which has surface wave velocity of approximately 3 km/sec near surface and is slower than the surrounding area.

4.0.1 Future direction and suggestions

In chapter 2 we highlight Lake Microseism as an intriguing possibility after reviewing various known mechanisms for regional noise generation. The origin of this noise source remains inconclusive, though it is clear that the energy associated with the excitation can reach broadband seismic receivers several hundred kilometres away. Our hypothesis is aided by the absence of known microseismic sources/mechanisms in the region and the spectral content of the asymmetric SC-CFs, while limited observational and theoretical support, moderate source location uncertainty and interfering ocean microseism are legitimate concerns. Improved source location and characterization [e.g., Schimmel et al., 2011], as well as a greater understanding of lake hydrodynamics, will be necessary to reliably determine the nature of the observed microseisms in southern-central Alberta.

A velocity model inverted from cross correlation of the vertical components of broadband seismic recordings are presented in chapter 3. Noise-correlation has been extensively utilized to map the seismic structure of subsurface down to the upper mantle. The effectiveness of noise-correlation is heavily dependent on station density and overlapping operating time of station pairs. Overall, the results of noise tomography reveal complex crustal structures and domains in Alberta. While the origins of many observed features remain largely speculative, the improved data coverage based on regional arrays does, and will continue to, provide critical insights to the formation and evolution of the Alberta basement structures. Despite the discoveries revealed by our current model, the seismic velocities are not well constrained in the areas to the north of latitude 52 degree, due to limited station coverage in northern part of the province. The resolution in northern part of our model will receive a significant boost should more stations, permanent or temporary, be deployed in region near Fort McMurray and Peace River. In addition to denser data coverage, the

presented velocity model can be refined through an improved 3D inversion process. In this study, 2-D ray path is assumed between two correlated stations. Therefore, only 2-D sensitivity kernels are computed with various idealizations including spatial uniformity and zero attenuation. A true 3D inversion can be achieved based on the consideration of the Fresnel volumes of seismic waves [Liu and Tromp, 2006; Chen *et al.*, 2007; Tromp *et al.*, 2010], a more refined 3D velocity model can be attained for better vertical resolutions.

Aside from the improvement of velocity model, anisotropy should also be considered when developing the tectonic model for the region. Most of the domains discussed in chapter 3 are highly deformed since their formation as early as Precambrian. Due to the common presence of compression, delamination and sedimentation, the crust in those domains could be highly anisotropic. Detailed analysis on the anisotropy and isotropy of the crust in the area will yield better constraint on the tectonic interaction among those domains and therefore lead to a better understanding on the history and evolution of the region. We compared the inverted travel time maps computed from Vertical Component and Radial Component. (Figure 4.1). Lacombe domain, which is inundated by thick sedimentary materials, displays first order differences between V_v and V_h . Aside from heavy sedimentations, Lacombe domain is also positioned between Wabamun domain and LVB, two domains which had been involved in a subduction process during the Paleoproterozoic. Another area of strong anisotropy is the east of MHB along with the nearby VS and Eyehill high. The geographic location of this anomaly overlaps with the reported HCLC from SAREX [Clowes *et al.*, 2002] experiment. The intrusion of the HCLC from Wyoming province could be potentially responsible for this anomalous anisotropic pattern. Also, it's speculative that THO, which collided with Hearne province in an era coeval with the collision between Hearne and Wabamun domain, may also be associated with this anisotropic pattern. Resolution-wise, this map is computed by

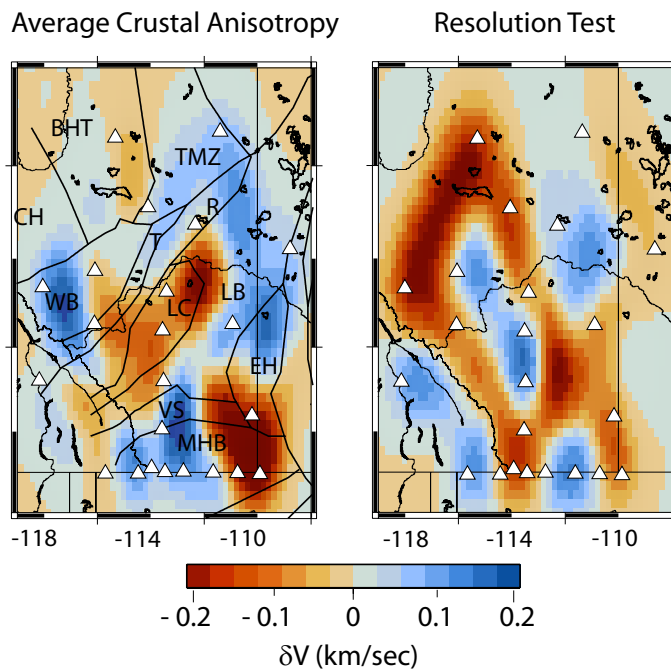


Figure 4.1: Anisotropy of crust. The anisotropy is quantified as $V_v - V_h$, while V_v is the velocity inverted from vertical component and V_h is inverted from radial component. The black lines denote the reported boundaries between known tectonic blocks [Ross *et al.*, 1991]. CRANE and CNSN stations used in this study are represented by white triangles.

subtracting inverted velocity models independently computed from vertical components and radial components. This approach is limited by the accumulated errors from two independent inversion practises that lead to high uncertainties in the resolved amplitude of anisotropy. Besides, directionalities of station pairs used in this study are not considered due the limited quality SCCFs for inversion. A more advanced adjoint tomographic scheme and a greater number of seismic recordings for cross-correlation will be beneficial in providing a better constrained anisotropic model.

Bibliography

- Ardhuin, F., E. Stutzmann, M. Schimmel, and A. Mangeney (2011), Ocean wave sources of seismic noise, *Journal of Geophysical Research*, *116*(C9), C09,004, doi:10.1029/2011JC006952.
- Aspler, L. B., J. R. Chiarenzelli, and V. J. McNicoll (2002), Paleoproterozoic basement-cover infolding and thick-skinned thrusting in Hearne domain, Nunavut, Canada: intracratonic response to Trans-Hudson orogen, *Precambrian Research*, *116*, 331–354.
- Audet, P., A. M. Jellinek, and H. Uno (2007), Mechanical controls on the deformation of continents at convergent margins, *Earth and Planetary Science Letters*, *264*(1-2), 151–166, doi:10.1016/j.epsl.2007.09.024.
- Aulbach, S., W. L. Griffin, S. Y. O'Reilly, and T. E. McCandless (2004), Genesis and evolution of the lithospheric mantle beneath the Buffalo Head Terrane, Alberta (Canada), *Lithos*, *77*(1-4), 413–451, doi:10.1016/j.lithos.2004.04.020.
- Bachu, S. (1993), Basement heat flow in the Western Canada sedimentary basin, *Tectonophysics*, *222*(1), 119–133.
- Banas, A., T. Stachel, K. Muehlenbachs, and T. E. McCandless (2007), Diamonds from the Buffalo Head Hills, Alberta: Formation in a non-conventional setting, *Lithos*, *93*(1-2), 199–213, doi:10.1016/j.lithos.2006.07.001.

- Barton, P. J. (1986), The relationship between seismic velocity and density in the continental crust useful constraint?, *Geophysical Journal of the Royal Astronomical Society*, pp. 195–208.
- Bassin, C., G. Laske, and G. Masters (2000), The current limits of resolution for surface wave tomography in North America, *EOS Trans. AGU.*, 81.
- Beaumont, C., P. Fullsack, and J. Hamilton (1994), Styles of crustal deformation in compressional orogens caused by subduction of the underlying lithosphere, *Tectonophysics*, 232(1-4), 119–132, doi:10.1016/0040-1951(94)90079-5.
- Bensen, G. D., and M. H. Ritzwoller (2008), Broadband ambient noise surface wave tomography across the United States, *J. geophys. Res.*, 113(December 2007), 1–21, doi:10.1029/2007JB005248.
- Bensen, G. D., M. H. Ritzwoller, M. P. Barmin, A. L. Levshin, F. Lin, M. P. Moschetti, N. M. Shapiro, and Y. Yang (2007a), Processing seismic ambient noise data to obtain reliable broad-band surface wave dispersion measurements, *Geophysical Journal International*, 169(3), 1239–1260, doi:10.1111/j.1365-246X.2007.03374.x.
- Bensen, G. D., M. H. Ritzwoller, M. P. Barmin, A. L. Levshin, F. Lin, M. P. Moschetti, N. M. Shapiro, and Y. Yang (2007b), Processing seismic ambient noise data to obtain reliable broad-band surface wave dispersion measurements, *Geophysical Journal International*, 169(3), 1239–1260, doi:10.1111/j.1365-246X.2007.03374.x.
- Berman, R. G., and H. H. Bostock (1997), Metamorphism in the northern Taltson magmatic zone, Northwest Territories, *The Canadian Mineralogist*, 35(5), 1069–1091.

- Berman, R. G., W. J. Davis, and S. Pehrsson (2007), Collisional Snowbird tectonic zone resurrected: Growth of Laurentia during the 1.9 Ga accretionary phase of the Hudsonian orogeny, *Geology*, 35(10), 911–914, doi:10.1130/G23771A.1.
- Bickford, M. E., K. D. Collerson, and J. F. Lewry (1994), Crustal history of the Rae and Hearne provinces, southwestern Canadian Shield, Saskatchewan: constraints from geochronologic and isotopic data, *Precambrian research*, 68, 1–21.
- Boerner, D. E. (1999), Electrical Conductivity in the Precambrian Lithosphere of Western Canada, *Science*, 283(5402), 668–670, doi:10.1126/science.283.5402.668.
- Boerner, D. E., R. D. Kurtz, and J. A. Craven (1995), Buried Proterozoic foredeep under the Western Canada Sedimentary Basin?, *Geology*, 23(4), 297–301, doi:10.1130/0091-7613(1995)0230297:BPFUTW2.3.CO;2.
- Boerner, D. E., J. A. Craven, R. D. Kurtz, G. M. Ross, and F. W. Jones (1998), The Great Falls Tectonic Zone: suture or intracontinental shear zone?, *Canadian Journal of Earth Sciences*, 35(2), 175–183.
- Boerner, D. E., R. D. Kurtz, J. A. Craven, G. M. Ross, and F. W. Jones (2000), A synthesis of electromagnetic studies in the Lithoprobe Alberta Basement Transect: constraints on Paleoproterozoic indentation tectonics, *Canadian Journal of Earth Sciences*, 37(11), 1509–1534, doi:10.1139/e00-063.
- Bouzidi, Y., and D. R. Schmitt (2002), Depth migration of deep seismic reflection profiles: crustal thickness variations in Alberta, *Canadian Journal of Earth Sciences*, 350, 331–350, doi:10.1139/E01-080.
- Brocher, T. M. (2005), Empirical Relations between Elastic Wavespeeds and Den-

- sity in the Earth's Crust, *Bulletin of the Seismological Society of America*, 95(6), 2081–2092, doi:10.1785/0120050077.
- Brooker, E. W., and R. B. Peck (1994), Rational design treatment of slides in over-consolidated clays and clay shales, *International Journal of Rock Mechanics and Mining Sciences & Geomechanics Abstracts*, 31(3), 159, doi:10.1016/0148-9062(94)90782-X.
- Brzak, K., Y. J. Gu, A. Ökeler, M. Steckler, and A. Lerner-Lam (2009), Migration imaging and forward modeling of microseismic noise sources near southern Italy, *Geochemistry Geophysics Geosystems*, 10(1), Q01,012, doi:10.1029/2008GC002234.
- Burwash, R. . A., T. Chacko, K. Muehlenbachs, and Y. Bouzidi (2000), Oxygen isotope systematics of the Precambrian basement of Alberta: implications for Paleoproterozoic and Phanerozoic tectonics in northwestern Alberta, *Canadian Journal of Earth Sciences*, 37(11), 1611–1628, doi:10.1139/e00-090.
- Burwash, R. A., and R. R. Culbert (1976), Multivariate geochemical and mineral patterns in the Precambrian basement of western Canada, *Canadian Journal of Earth Sciences*, 13(1), 1–18, doi:10.1139/e76-001.
- Burwash, R. A., and J. Krupička (1969), Cratonic reactivation in the Precambrian basement of western Canada. I. Deformation and chemistry, *Canadian Journal of Earth Sciences*, 6(6), 1381–1395, doi:10.1139/e69-140.
- Burwash, R. A., and J. Krupička (1970), Cratonic reactivation in the Precambrian basement of western Canada. Part II. Metasomatism and isostasy, *Canadian Journal of Earth Sciences*, 7(5), 1275–1294, doi:10.1139/e70-120.

- Burwash, R. A., and J. Krupička (2000), Metamorphic evolution of the Precambrian basement of Alberta, *The Canadian Mineralogist*, 38, 423–434.
- Burwash, R. A., and K. Muehlenbachs (1997), Tectonic setting of eastern Alberta basement granites inferred from Pearce trace element discrimination diagrams, *LITHOPROBE Alberta Basement Transects: Report of Transect Workshop, Calgary*, pp. 35–49.
- Burwash, R. A., J. Krupicka, and R. R. Culbert (1973), Cratonic reactivation in the Precambrian basement of western Canada. III. Crustal evolution, *Canadian Journal of Earth Sciences*, 10(2), 283–291, doi:10.1139/e73-025.
- Canil, D., D. J. Schulze, D. Hall, B. C. Hearn Jr, and S. M. Milliken (2003), Lithospheric roots beneath western Laurentia: the geochemical signal in mantle garnets, *Canadian Journal of Earth Sciences*, 40(8), 1027–1051, doi:10.1139/E03-003.
- Carlson, S. M., W. D. Hillier, and C. T. Hood (1999), The Buffalo Hills kimberlites: a newly-discovered diamondiferous kimberlite province in north-central Alberta, Canada, *8th International Kimberlite Conference*, 1, 109–116.
- Cassidy, J. F. (1995), A comparison of the receiver structure beneath stations of the Canadian National Seismograph Network, *Canadian Journal of Earth Sciences*, 32, 938–951.
- Chen, P., L. Zhao, and T. H. Jordan (2007), Full 3D Tomography for the Crustal Structure of the Los Angeles Region, *Bulletin of the Seismological Society of America*, 97(4), 1094–1120, doi:10.1785/0120060222.
- Chevrot, S., and M. Sylvander (2007), Source locations of secondary microseisms

- in western Europe: Evidence for both coastal and pelagic sources, *Journal of Geophysical Research*, 112, B05,301.
- Choy, G. L., V. F. Cormier, and R. Kind (1980), A comparison of synthetic seismograms of core phases generated by the full wave theory and by the reflectivity method, *Journal of the Royal Astronomical Society*, 61(1), 21–39.
- Christensen, N. I. (1979), Compressional wave velocities in rocks at high temperatures and pressures, critical thermal gradients, and crustal low-velocity zones, *Journal of geophysical research*, 84(B12), 6849–6857.
- Clevede, E., and C. Megnin (2000), Seismic waveform modeling and surface wave tomography in a three-dimensional Earth: asymptotic and non-asymptotic approaches, *Physics of the Earth and Planetary Interiors*, 119(1-2), 37–56, doi:10.1016/s0031-9201(99)00152-1.
- Clowes, R. M., C. A. Zelt, J. R. Amor, and R. M. Ellis (1995), Lithospheric structure in the southern Canadian Cordillera from a network of seismic refraction lines, *Canadian Journal of Earth Sciences*, 32, 1485–1513.
- Clowes, R. M., M. J. A. Burianyk, A. R. Gorman, and E. R. Kanasewich (2002), Crustal velocity structure from SAREX, the southern Alberta refraction experiment, *Canadian Journal of Earth Sciences*, 39(3), 351–373, doi:10.1139/E01-070.
- Contenti, S., Y. J. Gu, and M. D. Sacchi (2012), Upper mantle transition from cratons to terranes in western Canada, *Submitted to Journal of Geophysical Research*.
- Cook, F. A., and A. J. Van der Velden (1993), Proterozoic crustal transition be-

- neath the Western Canada sedimentary basin, *Geology*, 21(9), 785–788, doi: 10.1130/0091-7613(1993)021;0785.
- Cook, F. A., and D. J. White (2010), How the crust meets the mantle: Lithoprobe perspectives on the Mohorovicic discontinuity and crustmantle transition, *Canadian Journal of Earth Sciences*, 47(4), 315–351, doi:10.1139/E09-076.
- Courtier, A. M., J. B. Gaherty, and J. Revenaugh (2010), Seismic anisotropy associated with continental lithosphere accretion beneath the CANOE array, northwestern Canada, *Geology*, 38(10), 887–890, doi:10.1130/G31120.1.
- Crocker, C. H., K. D. Collerson, J. F. Lewry, and M. E. Bickford (1993), Sm-Nd, U-Pb, and Rb-Sr geochronology and lithostructural relationships in the southwestern Rae province: constraints on crustal assembly in the western Canadian shield, *Precambrian research*, 61, 27–50.
- Dalton, C. A., J. B. Gaherty, and A. M. Courtier (2011), Crustal V S structure in northwestern Canada: Imaging the Cordillera-craton transition with ambient noise tomography, *Journal of Geophysical Research*, 116(B12), 1–30, doi: 10.1029/2011JB008499.
- Davies, M. R., R. C. Paulen, and A. S. Hickin (2005), Inventory of Holocene landslides, Peace River area, Alberta (NTS 84C), *Tech. rep.*, Alberta Energy Utility Board, EUB/AGS Geo-Note, Edmonton, Alberta, Canada.
- Davies, R. . M., W. L. Griffin, S. Y. O'Reilly, and T. E. McCandless (2004), Inclusions in diamonds from the K14 and K10 kimberlites, Buffalo Hills, Alberta, Canada: diamond growth in a plume?, *Lithos*, 77(1-4), 99–111, doi: 10.1016/j.lithos.2004.04.008.
- De, S. K., T. Chacko, R. A. Creaser, and K. Muehlenbachs (2000), Geochemical

- and Nd-Pb-O isotope systematics of granites from the Taltson Magmatic Zone, NE Alberta: implications for early Proterozoic tectonics in western, *Precambrian Research*, 102(3), 221–249.
- Dietrich, J. R. (1999), Seismic stratigraphy and structure of the lower Paleozoic, central Alberta LITHOPROBE transect, *Bulletin of canadian petroleum geology*, 47(4), 362–374.
- Eaton, D. W., and J. F. Cassidy (1996), A relic Proterozoic subduction zone in western Canada: New evidence from seismic reflection and receiver function data, *Geophysical research letters*, 23(25), 3791–3794.
- Eaton, D. W., G. M. Ross, and J. Hope (1999a), The rise and fall of a cratonic arch: A regional seismic perspective on the Peace River Arch, Alberta, *Bulletin of canadian petroleum geology*, 47(4), 346–361.
- Eaton, D. W., G. M. Ross, and R. M. Clowes (1999b), Seismic-reflection and potential-field studies of the Vulcan structure, western Canada: A Paleoproterozoic Pyrenees?, *Journal of Geophysical Research*, 104(B10), 23,255–23,269, doi:10.1029/1999JB900204.
- Eaton, D. W., G. M. Ross, F. A. Cook, and A. VanderVelden (2000), Seismic imaging of the upper mantle beneath the Rocky Mountain foreland, southwestern Alberta, *Canadian Journal of Earth Sciences*, 37(11), 1493–1507, doi: 10.1139/e00-068.
- Eccles, D. R., and L. M. Heaman (2003), Petrogenetic considerations for the late Cretaceous northern Alberta kimberlite province, *8th International Kimberlite Conference Abstract*, pp. 1–5.

- Edwards, D. J., and R. J. Brown (1999), Understanding the influence of Precambrian crystalline basement on Upper Devonian carbonates in central Alberta from a geophysical perspective, *Bulletin of Canadian Petroleum Geology*, 47(4), 412–438.
- English, J. M., and S. T. Johnston (2004), The Laramide Orogeny: what were the driving forces?, *International Geology Review*, 46(9), 833–838, doi:10.2747/0020-6814.46.9.833.
- Ersan, T., U. Martyn, and D. Pana (2009), Deep electrical structure of northern Alberta (Canada): implications for diamond exploration, *Canadian Journal of Earth Sciences*, 46(2), 139–154, doi:10.1139/E09-009.
- Flowers, R. M., S. A. Bowring, and M. L. Williams (2006), Timescales and significance of high-pressure, high-temperature metamorphism and mafic dike anatexis, Snowbird tectonic zone, Canada, *Contributions to Mineralogy and Petrology*, 151(5), 558–581, doi:10.1007/s00410-006-0066-7.
- Flück, P., R. D. Hyndman, and C. Lowe (2003), Effective elastic thickness of the lithosphere in western Canada, *Journal of Geophysical Research*, 108(B9), 2430, doi:10.1029/2002JB002201.
- Fouch, M. J., and D. E. James (2004), Mantle seismic structure beneath the Kaapvaal and Zimbabwe Cratons, *South African Journal of Earth Sciences*, 107(1-2), 33–44, doi:10.2113/107.1-2.33.
- Frederiksen, A. W., M. G. Bostock, and J. F. Cassidy (2001), S-wave velocity structure of the Canadian upper mantle, *Physics of the Earth and Planetary Interiors*, 124(3-4), 175–191, doi:10.1016/S0031-9201(01)00194-7.
- French, S. W., K. M. Fischer, E. M. Syracuse, and M. E. Wysession (2009), Crustal

- structure beneath the FloridatoEdmonton broadband seismometer array, *Geophysical Research Letters*, 36(8), 1–6, doi:10.1029/2008GL036331.
- Friedmann, S. J. (2003), Granular memory and its effect on the triggering and distribution of rock avalanche events, *Journal of Geophysical Research*, 108(B8), 2380, doi:10.1029/2002JB002174.
- Frost, C. D., and R. A. Burwash (1986), Nd evidence for extensive Archean basement in the western Churchill Province, Canada, *Canadian Journal of Earth Sciences*, 23(9), 1433–1437.
- Fuchs, K., and G. Müller (2007), Computation of synthetic seismograms with the reflectivity method and comparison with observations, *Journal of the Royal Astronomical Society*, 23(4), 417–433, doi:10.1111/j.1365-246X.1971.tb01834.x.
- Gerstoft, P., and T. Tanimoto (2007), A year of microseisms in southern California, *Geophysical Research Letters*, 34(20), L20,304, doi:10.1029/2007GL031091.
- Godey, S., R. Snieder, A. Villasenor, and H. M. Benz (2003), Surface wave tomography of North America and the Caribbean using global and regional broad-band networks: phase velocity maps and limitations of ray theory, *Geophysical Journal International*, 152, 620–632.
- Gorman, A. R., R. M. Clowes, R. M. Ellis, T. J. Henstock, G. D. Spence, G. R. Keller, A. Levander, C. M. Snelson, M. J. A. Burianyk, E. R. Kanasewich, and Others (2002), Deep Probe: imaging the roots of western North America, *Canadian Journal of Earth Sciences*, 39(3), 375–398, doi:10.1139/E01-064.
- Grand, S. P., R. D. van der Hilst, and W. Sri (1997), High resolution global tomography: a snapshot of convection in the Earth, *Geological Society of America Today*, 7(4), 1–7.

- Gu, Y. (2010), *Arrays and array methods in global seismology*, Springer Netherlands, Dordrecht, doi:10.1007/978-90-481-3680-3.
- Gu, Y. J. (2006), Probing the history of the Mathematician paleoplate using surface waves, *Tectonophysics*, 424(1-2), 41–51, doi:10.1016/j.tecto.2006.06.002.
- Gu, Y. J., and L. Shen (2012), Microseismic Noise from Large Ice Covered Lakes?, *Bulletin of the Seismological Society of America*, 102(3), 1155–1166, doi:10.1785/0120100010.
- Gu, Y. J., S. C. Webb, A. Lerner-Lam, and J. B. Gaherty (2005), Upper mantle structure beneath the eastern Pacific Ocean ridges, *Journal of Geophysical Research*, 110(B6), 1–18, doi:10.1029/2004JB003381.
- Gu, Y. J., C. Dublanko, A. Lerner-Lam, K. Brzak, and M. Steckler (2007), Probing the sources of ambient seismic noise near the coasts of southern Italy, *Geophysical Research Letters*, 34(22), L22,315, doi:10.1029/2007GL031967.
- Gu, Y. J., A. Ökeler, S. Contenti, and K. Kocon (2009), Broadband seismic array deployment and data analysis in Alberta, *CSEG Recorder*, September, 37–44.
- Gu, Y. J., A. Okeler, L. Shen, and S. Contenti (2011), the canadian rockies and alberta network (crane): new constraints on the rockies and western canada sedimentary basin, *Seismological Research Letter*, 82(4), 575–588, doi:10.1785/gssrl.
- Gutenberg, B. (1951), Observation and theory of microseisms, *Compendium of Meteorology*, (American Meteorology Society, Providence, Rhode Island), 1303–1311.
- Hanmer, S., M. Williams, and C. Kopf (1995), Striding-Athabasca mylonite zone: implications for the Archean and Early Proterozoic tectonics of the western

- Canadian Shield, *Canadian Journal of Earth Sciences*, 32(2), 178–196, doi:10.1139/e95-015.
- Hasselmann, K. (1963), A statistical analysis of the generation of microseisms, *Reviews of Geophysics*, 1(2), 177, doi:10.1029/RG001i002p00177.
- Haubrich, R. A., and K. McCamy (1969), Microseisms: Coastal and pelagic sources, *Reviews of Geophysics*, 7(3), 539, doi:10.1029/RG007i003p00539.
- Henstock, T. J., A. Levander, C. M. Snelson, and G. R. Keller (1998), Probing the Archean and Proterozoic lithosphere of western North America, *Geological Society of America Today*, 8(7), 1–5.
- Hoffman, P. F. (1988), United Plates of America, the birth of a craton-Early Proterozoic assembly and growth of Laurentia, *Annual Review of Earth and Planetary Sciences*, 16, 543–603.
- Hoffman, P. F. (1989), Precambrian geology and tectonic history of North America, *The Geological Society of America, A*(The Geology of North America-An overview), 447–512.
- Hoffman, P. F. (1990), Subdivision of the Churchill Province and Extent of the Tran-Hudson Orogen, *Geological Society of Canada, Special pa*(37), 15–39.
- Holbrook, W. S., W. D. Mooney, and N. I. Christensen (1992), The seismic velocity structure of the deep continental crust, *Continental lower crust*, 1(1987), 1–43.
- Hood, C. T. S., and T. E. McCandless (2004), Systematic variations in xenocryst mineral composition at the province scale, Buffalo Hills kimberlites, Alberta, Canada, *Lithos*, 77(1-4), 733–747, doi:10.1016/j.lithos.2004.03.015.

- Hope, J., and D. Eaton (2002), Crustal structure beneath the Western Canada Sedimentary Basin: Constraints from gravity and magnetic modelling, *Canadian Journal of Earth Sciences*, 39(3), 291–312, doi:10.1139/E01-060.
- Huang, H., H. Yao, and R. D. van der Hilst (2010), Radial anisotropy in the crust of SE Tibet and SW China from ambient noise interferometry, *Geophysical Research Letters*, 37(21), 1–5, doi:10.1029/2010GL044981.
- Hughes, B. (1976), Estimates of underwater sound (and infrasound) produced by nonlinearly interacting ocean waves, *The Journal of the Acoustical Society of America*, 60(5), 1032, doi:10.1121/1.381203.
- Hyndman, R. D., and T. J. Lewis (1999), Geophysical consequences of the Cordillera Craton thermal transition in southwestern Canada, *Tectonophysics*, 306(3-4), 397–422, doi:10.1016/S0040-1951(99)00068-2.
- Janse, A. J. A. (1994), Is Clifford's rule still valid? Affirmative examples from around the world, *Fifth International Kimberlite Conference*, 2, 215–235.
- Jones, A. G. (2002), Magnetotelluric and teleseismic study across the Snowbird Tectonic Zone, Canadian Shield: A Neoproterozoic mantle suture?, *Geophysical Research Letters*, 29(17), 17–20, doi:10.1029/2002GL015359.
- Jones, A. G., and J. Ledo (2005), The electrical resistivity structure of Archean to Tertiary lithosphere along 3200 km of SNORCLE profiles, northwestern Canada, *Canadian Journal of Earth Sciences*, 42(6), 1257–1275, doi:10.1139/e05-080.
- Kanasewich, E., R. Clowes, and C. McCloughan (1969), A buried Precambrian rift in western Canada, *Tectonophysics*, 8(4-6), 513–527, doi:10.1016/0040-1951(69)90051-1.

- Kanasewich, E. R., M. J. A. Burianyk, and G. Dubuc (1995), Three-Dimensional Seismic Reflection Studies of the Alberta Basement, *Canadian Journal of Exploration Geophysics*, 31, 1–10.
- Kedar, S., M. Longuet-Higgins, F. Webb, N. Graham, R. Clayton, and C. Jones (2008), The origin of deep ocean microseisms in the North Atlantic Ocean, *Proceedings of the Royal Society A: Mathematical, Physical and Engineering Sciences*, 464(2091), 777–793, doi:10.1098/rspa.2007.0277.
- Kelley, D. E. (1997), Convection in ice-covered lakes: effects on algal suspension, *Journal of Plankton Research*, 19(12), 1859–1880, doi:10.1093/plankt/19.12.1859.
- Kenney, B. C. (1991), Under-Ice Circulation and the Residence Time of a Shallow Bay, *Canadian Journal of Fisheries and Aquatic Sciences*, 48(1), 152–162, doi:10.1139/f91-021.
- Kenney, B. C. (1996), Physical limnological processes under ice, *Hydrobiologia*, 322(1-3), 85–90, doi:10.1007/BF00031810.
- Kerman, B. R., and R. F. Mereu (1993), Wind induced microseisms from Lake Ontario, *Atmosphere-Ocean*, 31(4), 501–516, doi:10.1080/07055900.1993.9649483.
- Koper, K. D., K. Seats, and H. Benz (2010), On the Composition of Earth's Short-Period Seismic Noise Field, *Bulletin of the Seismological Society of America*, 100(2), 606–617, doi:10.1785/0120090120.
- Kvarnäs, H. (2001), Morphometry and hydrology of the four large lakes of Sweden., *Ambio*, 30(8), 467–74.

- Lemieux, S., G. M. Ross, and F. A. Cook (2000), Crustal geometry and tectonic evolution of the Archean crystalline basement beneath the southern Alberta Plains, from new seismic reflection and potential-field studies, *Canadian Journal of Earth Sciences*, 37(11), 1473–1491, doi:10.1139/e00-065.
- Lewis, T. J., R. D. Hyndman, and P. Flück (2003), Heat flow, heat generation, and crustal temperatures in the northern Canadian Cordillera: thermal control of tectonics, *Journal of Geophysical Research*, 108(B6), 2316, doi:10.1029/2002JB002090.
- Lewry, J. F., and T. I. Sibbald (1980), Thermotectonic evolution of the Churchill Province in northern Saskatchewan, *Tectonophysics*, 68, 45–82.
- Lin, F.-C., M. P. Moschetti, and M. H. Ritzwoller (2008), Surface wave tomography of the western United States from ambient seismic noise: Rayleigh and Love wave phase velocity maps, *Geophysical Journal International*, 173(1), 281–298, doi:10.1111/j.1365-246X.2008.03720.x.
- Liu, L., M. Gurnis, M. Seton, J. Saleeby, R. D. Müller, and J. M. Jackson (2010), The role of oceanic plateau subduction in the Laramide orogeny, *Nature Geoscience*, 3(5), 353–357, doi:10.1038/ngeo829.
- Liu, Q., and J. Tromp (2006), Finite-Frequency Kernels Based on Adjoint Methods, *Bulletin of the Seismological Society of America*, 96(6), 2383–2397, doi:10.1785/0120060041.
- Livaccari, R. F., K. Burke, and A. M. C. Sengor (1981), Was the Laramide orogeny related to subduction of an oceanic plateau?, *Nature*, 289, 276–278.
- Lobkis, O. I., and R. L. Weaver (2001), On the emergence of the Greens function

- in the correlations of a diffuse field, *The Journal of the Acoustical Society of America*, 110(6), 3011, doi:10.1121/1.1417528.
- Longuet-Higgins, M. (1950), A theory of the origin of microseism, *Philos. Trans. Roy. Soc. Lond*, 243, 1–35.
- Lynch, J. (1952), The Great Lakes, a source of two-second frontal microseisms, *Transactions, American Geophysical Union*, 19, 177–182.
- Mahan, K. H., and M. L. Williams (2005), Reconstruction of a large deep-crustal terrane: Implications for the Snowbird tectonic zone and early growth of Laurentia, *Geology*, 33(5), 385, doi:10.1130/G21273.1.
- Majorowicz, J., and M. . C. Moore (2008), Enhanced Geothermal Systems (EGS) Potential in the Alberta Basin, *Tech. Rep. July*, University of Calgary, Institute for Sustainability, Energy, Environment and Economy, Calgary.
- Mansour, M. F. (2009), Characteristic behaviour of slow moving slides, Ph.D. thesis, University of Alberta, Alberta Canada.
- Marone, F., and B. Romanowicz (2007), Non-linear crustal corrections in high-resolution regional waveform seismic tomography, *Geophysical Journal International*, 170(1), 460–467, doi:10.1111/j.1365-246X.2007.03399.x.
- Maxson, J., and B. Tikoff (1996), Hit-and-run collision model for the Laramide orogeny, western United States, *Geology*, 24(11), 968–972.
- McDonough, M. R., V. J. McNicoll, E. M. Schetselaar, and T. W. Grover (2000), Geochronological and kinematic constraints on crustal shortening and escape in a two-sided oblique-slip collisional and magmatic orogen, Paleoproterozoic Taltson magmatic zone, northeastern Alberta, *Canadian Journal of Earth Sciences*, 37(11), 1549–1573, doi:10.1139/e00-089.

- McNicoll, V. J., R. J. Thériault, and M. R. McDonough (2000), Taltson basement gneissic rocks: UPb and Nd isotopic constraints on the basement to the Paleoproterozoic Taltson magmatic zone, northeastern Alberta, *Canadian Journal of Earth Sciences*, 37(11), 1575–1596, doi:10.1139/e00-034.
- Mercier, J.-P., M. G. Bostock, P. Audet, J. B. Gaherty, E. J. Garnero, and J. Revenaugh (2008), The teleseismic signature of fossil subduction: Northwestern Canada, *Journal of Geophysical Research*, 113(B4), 1–16, doi:10.1029/2007JB005127.
- Mercier, J.-P., M. G. Bostock, J. F. Cassidy, K. Dueker, J. B. Gaherty, E. J. Garnero, J. Revenaugh, and G. Zandt (2009), Body-wave tomography of western Canada, *Tectonophysics*, 475(3-4), 480–492, doi:10.1016/j.tecto.2009.05.030.
- Monger, J. W. H., R. A. Price, and D. J. Tempelman-Kluit (1982), Tectonic accretion and the origin of the two major metamorphic and plutonic belts in the Canadian Cordillera, *Geology*, 10(2), 70–75.
- Morgan, A. J., R. C. Paulen, and C. R. Froese (2008), Ancestral buried valleys of the Peace River: Effects on the town of Peace River, in *Proceed. 61st Can. Geotech.*, pp. 1219–1226.
- Mueller, P. A., A. L. Heatherington, D. M. Kelly, J. L. Wooden, and D. W. Mogk (2002), Paleoproterozoic crust within the Great Falls tectonic zone: Implications for the assembly of southern Laurentia, *Geology*, 30(2), 127–130.
- Németh, B., R. M. Clowes, and Z. Hajnal (2005), Lithospheric structure of the Trans-Hudson Orogen from seismic refraction-wide-angle reflection studies, *Canadian Journal of Earth Sciences*, 42(4), 435–456, doi:10.1139/E05-032.
- Nettles, M., and A. M. Dziewonski (2008), Radially anisotropic shear velocity

- structure of the upper mantle globally and beneath North America, *Journal of Geophysical Research*, 113(B2), B02,303, doi:10.1029/2006JB004819.
- Nishida, K., J.-P. Montagner, and H. Kawakatsu (2009), Global surface wave tomography using seismic hum., *Science (New York, N.Y.)*, 326(5949), 112, doi: 10.1126/science.1176389.
- O'Connell, D. R. H. (2007), Concrete dams as seismic imaging sources, *Geophysical Research Letters*, 34(20), L20,307, doi:10.1029/2007GL031219.
- Ökeler, A., Y. J. Gu, A. Lerner-Lam, and M. S. Steckler (2009), Seismic structure of the southern Apennines as revealed by waveform modelling of regional surface waves, *Geophysical Journal International*, 178(3), 1473–1492, doi: 10.1111/j.1365-246X.2009.04229.x.
- Patterson, J., and P. Hamblin (1988), Thermal simulation of a lake with winter ice cover, *Limnology and Oceanography*, 33, 323–338.
- Paul, A. (2005), Empirical synthesis of time-asymmetrical Green functions from the correlation of coda waves, doi:10.1029/2004JB003521.
- Pedrazzini, A., and M. Jaboyedoff (2008), Structures and failure mechanisms analysis of Turtle Mountain, in *Proceed. 4th Can. Conf. Geohazards*, p. 594.
- Pilkington, M., W. F. Miles, G. M. Ross, and W. R. Roest (2000), Potential-field signatures of buried Precambrian basement in the Western Canada Sedimentary Basin, *Canadian Journal of Earth Sciences*, 37(11), 1453–1471, doi: 10.1139/cjes-37-11-1453.
- Polzin, K. I., J. M. Toole, J. Ledwell, and R. W. Schmitt (1997), Spatial Variability of Turbulent Mixing in the Abyssal Ocean, *Science (New York, N.Y.)*, 276(5309), 93–6.

- Rawlinson, N., and M. Sambridge (2005), The fast marching method: an effective tool for tomographic imaging and tracking multiple phases in complex layered media, *Exploration Geophysics*, 36(4), 341–350, doi:10.1071/EG05341.
- Rhie, J., and B. Romanowicz (2006), A study of the relation between ocean storms and the Earth's hum, *Geochemistry Geophysics Geosystems*, 7(10), Q10,004, doi: 10.1029/2006GC001274.
- Ritzwoller, M. H., F.-C. Lin, and W. Shen (2011), Ambient noise tomography with a large seismic array, *Comptes Rendus Geoscience*, 343(8-9), 558–570, doi: 10.1016/j.crte.2011.03.007.
- Rogers, C. K., G. a. Lawrence, and P. F. Hamblin (1995), Observations and numerical simulation of a shallow ice-covered midlatitude lake, *Limnology and Oceanography*, 40(2), 374–385, doi:10.4319/lo.1995.40.2.0374.
- Ross, G. M. (2000), Introduction to special issue of Canadian Journal of Earth Sciences : The Alberta Basement Transect of Lithoprobe, *Canadian Journal of Earth Sciences*, 37(11), 1447–1452.
- Ross, G. M., and D. W. Eaton (1997), Winagami reflection sequence: Seismic evidence for postcollisional magmatism in the Proterozoic of western Canada, *Geology*, 25(3), 199–202.
- Ross, G. M., and D. W. Eaton (1999), Basement reactivation in the Alberta Basin: Observational constraints and mechanical rationale, *Bulletin of Canadian Petroleum Geology*, 47(4), 391–411.
- Ross, G. M., and D. W. Eaton (2002), Proterozoic tectonic accretion and growth of western Laurentia: results from Lithoprobe studies in northern Alberta, *Canadian Journal of Earth Sciences*, 39(3), 313–329, doi:10.1139/E01-081.

- Ross, G. M., R. R. Parrish, M. E. Villeneuve, and S. A. Bowring (1991), Geophysics and geochronology of the crystalline basement of the Alberta Basin, western Canada, *Canadian Journal of Earth Sciences*, 28(4), 512–522.
- Ross, G. M., B. Milkereit, D. Eaton, D. White, E. R. Kanasewich, and M. J. A. Buri- anyk (1995), Paleoproterozoic collisional orogen beneath the western Canada sedimentary basin imaged by Lithoprobe crustal seismic-reflection data, *Geol- ogy*, 23(3), 195–199.
- Ross, G. M., D. W. Eaton, D. E. Boerner, and W. Miles (2000), Tectonic entrapment and its role in the evolution of continental lithosphere: An example from the Precambrian of western Canada, *Tectonics*, 19(1), 116–134.
- Sabra, K. G., P. Gertoft, P. Roux, and W. A. Kuperman (2005a), Surface wave to- mography from microseisms in Southern California, *Geophysical Research Let- ters*, 32(14), 1–4, doi:10.1029/2005GL023155.
- Sabra, K. G., P. Gerstoft, and P. Roux (2005b), Extracting time-domain Green’s function estimates from ambient seismic noise, *Geophysical Research Letter*, 32, L03,310.
- Saygin, E., and B. L. N. Kennett (2010), Ambient seismic noise tomog- raphy of Australian continent, *Tectonophysics*, 481(1-4), 116–125, doi: 10.1016/j.tecto.2008.11.013.
- Saygin, E., and B. L. N. Kennett (2012), Crustal structure of Australia from ambient seismic noise tomography, *Journal of Geophysical Research*, 117(B1), 1–15, doi:10.1029/2011JB008403.
- Schimmel, M., E. Stutzmann, F. Arduin, and J. Gallart (2011), Polarized Earth’s

- ambient microseismic noise, *Geochemistry Geophysics Geosystems*, 12(7), Q07,014, doi:10.1029/2011GC003661.
- Schulte-Pelkum, V. (2004), Strong directivity of ocean-generated seismic noise, *Geochemistry Geophysics Geosystems*, 5(3), Q03,004, doi:10.1029/2003GC000520.
- Shapiro, N., and M. Campillo (2004), Emergence of broadband Rayleigh waves from correlations of the ambient seismic noise, *Geophysical Research Letters*, 31(7), 8–11, doi:10.1029/2004GL019491.
- Shapiro, N., M. Ritzwoller, and G. Bensen (2006), Source location of the 26 sec microseism from cross-correlations of ambient seismic noise, *Geophysical research letters*, 33(L18310), doi:10.1029/2005JB004237.
- Shapiro, N. M., M. Campillo, L. Stehly, and M. H. Ritzwoller (2005), High-resolution surface-wave tomography from ambient seismic noise., *Science*, 307(5715), 1615–1618, doi:10.1126/science.1108339.
- Shragge, J., M. G. Bostock, C. G. Bank, and R. M. Ellis (2002), Integrated teleseismic studies of the southern Alberta upper mantle, *Canadian Journal of Earth Sciences*, 39(3), 399–411, doi:10.1139/E01-084.
- Simons, F. J., A. Zielhuis, and R. D. van der Hilst (1999), The deep structure of the Australian continent from surface wave tomography, *Developments in Geotectonics*, 48(1-4), 17–43, doi:10.1016/S0024-4937(99)00041-9.
- Stehly, L., M. Campillo, and N. M. Shapiro (2006), A study of the seismic noise from its long-range correlation properties, *Journal of Geophysical Research*, 111(B10), B10,306, doi:10.1029/2005JB004237.

- Stein, S., and M. Wysession (2009), *An introduction to seismology, earthquakes, and earth structure*, Blackwell Publishing Ltd. 350 Main Street, Malden, MA0214805020, USA.
- Stern, V., and Y. J. Gu (2011), Documenting Alberta seismicity with BRTTs Antelope software, *5th Can. Conf. Geotech. Natural Hazard, Kelowna, British Columbia*, p. 7 pages.
- Suda, N., K. Nawa, and Y. Fukao (1998), Earth's background free oscillations, *Science (New York, N.Y.)*, 279(5359), 2089–91.
- Tanimoto, T., J. Um, K. Nishida, and N. Kobayashi (1998), Earth's continuous oscillations observed on seismically quiet days, *Geophysical Research Letters*, 25(10), 1553–1559, doi:10.1029/98GL01223.
- Tarantola, A. (2005), *Inverse problem theory and methods for model parameter estimation*, Society for Industrial and Applied Mathematics, 3600 University City Science Center, Philadelphia, PA.
- Thériault, R. J. (1992), Nd isotopic evolution of the Taltson Magmatic Zone, Northwest Territories, Canada: insights into Early Proterozoic accretion along the western margin of the, *The Journal of Geology*, 100(4), 465–475.
- Thériault, R. J., and G. M. Ross (1990), Nd isotopic evidence for crustal recycling in the ca. 2.0 Ga subsurface of western Canada, *Canadian Journal of Earth Sciences*, 28(1989), 1140–1147.
- Thomas, M. D., V. L. Sharpton, and R. A. F. Grieve (1987), Gravity patterns and Precambrian structure in the North American central plains, *Geology*, 15(6), 489–492.

- Tikku, A. A., D. C. McAdoo, M. S. Schenewerk, and E. C. Willoughby (2006), Temporal fluctuations of microseismic noise in Yellowstone's Upper Geyser Basin from a continuous gravity observation, *Geophysical Research Letters*, 33(11), L11,306, doi:10.1029/2006GL026113.
- Tromp, J., Y. Luo, S. Hanasoge, and D. Peter (2010), Noise cross-correlation sensitivity kernels, *Geophysical Journal International*, 183(2), 791–819, doi: 10.1111/j.1365-246X.2010.04721.x.
- Tsai, V. (2010), Strong directivity of ocean-generated seismic noise, *Geophysical Journal International*, (182), 1509–1514.
- Ugalde, H., and S. L. Underhay (2008), Evidence for basement fault reactivation in southern Alberta: an integrated topography and airborne magnetics approach, *Canadian Society of Exploration Geophysicists Recorder*, 33(Suppl 1), 32–38.
- Van Avendonk, H. J. a., W. S. Holbrook, D. Lizarralde, and P. Denyer (2011), Structure and serpentization of the subducting Cocos plate offshore Nicaragua and Costa Rica, *Geochemistry Geophysics Geosystems*, 12(6), Q06,009, doi: 10.1029/2011GC003592.
- van der Lee, S., and A. Frederiksen (2005), Surface wave tomography applied to the North American upper mantle, *Geophysical Monograph Series*, 157, 67–80, doi:10.1029/157GM05.
- Villeneuve, M. E., G. M. Ross, R. J. Thériault, W. Miles, R. R. Parrish, and J. Broome (1993), Geophysical subdivision and U-Pb geochronology of the crystalline basement of the Alberta Basin, Western Canada, *Geologica Survey of Canada, Bulletin*, 447, 86 pages.

- Webb, S. C. (2007), The Earth's 'hum' is driven by ocean waves over the continental shelves., doi:10.1038/nature05536.
- Welford, J. K., and R. M. Clowes (2006), Three-dimensional seismic reflection investigation of the upper crustal Winagami sill complex of northwestern Alberta, Canada, *Geophysical Journal International*, 166(1), 155–169, doi: 10.1111/j.1365-246X.2006.02805.x.
- Wessel, P., and W. H. F. Smith (1991), Free software helps map and display data, doi:10.1029/90EO00319.
- Yao, H., R. D. van der Hilst, and M. V. de Hoop (2006), Surface-wave array tomography in SE Tibet from ambient seismic noise and two-station analysis - I. Phase velocity maps, *Geophysical Journal International*, 166(2), 732–744, doi: 10.1111/j.1365-246X.2006.03028.x.
- Yilmaz, O. (2001), *Seismic data analysis: processing, inversion, and interpretation of seismic data, volume II, Investigations in Geophysics 10*, 2027 pp., Society of Exploration Geophysics, Tulsa, Oklahoma.
- Yuan, H., and B. Romanowicz (2010), Lithospheric layering in the North American craton., *Nature*, 466(7310), 1063–1068, doi:10.1038/nature09332.
- Zelt, C. A., and R. M. Ellis (1989), Seismic Structure of the Crust and Upper Mantle in the Peace River Arch Region, Canada, *Journal of Geophysical Research*, 94(B5), 5729–5744, doi:10.1029/JB094iB05p05729.
- Zelt, C. A., and D. J. White (1995), Crustal structure and tectonics of the southeastern Canadian Cordillera, *Journal of geophysical research*, 100(B12), 24,255–24,272.

Zhang, X., H. Paulssen, S. Lebedev, and T. Meier (2007), Surface wave tomography of the Gulf of California, *Geophysical Research Letter*, 34, L5305.

Appendix A

Appendix

A.1 List of Abbreviations

CRANE	Canadian Rockies and Alberta Network
CNSN	Canadian National Seismograph Network
WCSB	Western Canadian Sedimentary Basin
LSL	Lesser Slave Lake
SCCF(s)	stacked cross-correlation function(s)
CCF(s)	Cross-correlation function(s)
GSLSZ	Great Slave Lake shear zone
STZ	Snowbird Tectonic Zone
VS	Vulcan structure
BHT	Buffalo Head Terrane
TMZ	Taltson Magmatic Zone
THO	Trans-Hudson Orogen
EH	Eyehill High
LVB	Loverna Block
MHB	Medicine Hat Block
SNR	signal-to-noise ratio